Nanoscale

REVIEW

View Article Online
View Journal | View Issue

Cite this: *Nanoscale*, 2024, **16**, 11384

Advancements in mercury detection using surface-enhanced Raman spectroscopy (SERS) and ion-imprinted polymers (IIPs): a review

Frank Tukur,[a] Panesun Tukur,[a] Simona E. Hunyadi Murph *[b,c] and Jianjun Wei *[a]

Received 1st March 2024,
Accepted 29th May 2024

DOI: 10.1039/d4nr00886c

rsc.li/nanoscale

Mercury (Hg) contamination remains a major environmental concern primarily due to its presence at trace levels, making monitoring the concentration of Hg challenging. Sensitivity and selectivity are significant challenges in the development of mercury sensors. Surface-enhanced Raman spectroscopy (SERS) and ion-imprinted polymers (IIPs) are two distinct analytical methods developed and employed for mercury detection. In this review, we provide an overview of the key aspects of SERS and IIP methodologies, focusing on the recent advances in sensitivity and selectivity for mercury detection. By examining the critical parameters and challenges commonly encountered in this area of research, as reported in the literature, we present a set of recommendations. These recommendations cover solid and colloidal SERS substrates, appropriate Raman reporter/probe molecules, and customization of IIPs for mercury sensing and removal. Furthermore, we provide a perspective on the potential integration of SERS with IIPs to achieve enhanced sensitivity and selectivity in mercury detection. Our aim is to foster the establishment of a SERS-IIP hybrid method as a robust analytical tool for mercury detection across diverse fields.

1. Introduction

A quarter of the most lethal diseases afflicting humanity stem from the contact with water, soil, and air contaminated with pollutants, particularly heavy metals.[1] Among these heavy metal contaminants, mercury ranks as the third most perilous substance, contributing to over three billion individuals suffering from chemical poisoning, especially those who rely on seafood as their primary source of protein.[2,3] The UN Environmental Program and WHO state that 1.5 to 17 out of 1000 children are at risk of developing cognitive disorders due to the consumption of mercury-contaminated fish. Despite mercury's valuable industrial applications,[4,5] its extensive use has led to a 450% surge in atmospheric concentrations, contaminating water, air, and soil.[6] This results in severe health issues, including developmental disorders and damage to the nervous system and kidneys.[7,8] Given these alarming health implications, stringent permissible limits are set by regulatory agencies for mercury concentrations in the environment, such as 20 μg L^{-1} in blood or 0.002 mg L^{-1} in potable water resources (Table 1). These limits coupled with mercury's volatile nature make trace level detection challenging.

Most reported strategies concentrate on detecting the inorganic form of mercury (Hg^{2+}), paying less attention to quantifying the more toxicologically relevant methylmercury, probably owing to its high volatility that makes it difficult to handle.[9] Another persisting challenge is the inability of several novel Raman tags to discriminate between different mercury species. This challenge may arise from dynamic interconversion processes among various species, posing a significant

Table 1 Summary of mercury exposure limits in environmental and human samples

Sample	Exposure limit	Enacting body/ document	Ref.
Drinking water	0.002 mg L^{-1}	USEPA	12
Air	0.05 mg m^{-3}	—	13
Soil (farmland)	4 mg kg^{-1}	—	14
Soil (industrial site)	16 mg kg^{-1}	—	14
Industrial wastewater	0.05 μg mL^{-1}	—	15
Human blood	20 μg L^{-1}	ACGIH	13
Human urine	20 μg g^{-1} creatinine	OSHA	16

U.S. Environmental Protection Agency (US EPA), American Conference of Governmental Industrial Hygienists (ACGIH), Occupational Safety and Health Administration (OSHA).

---

[a] The Department of Nanoscience, Joint School of Nanoscience and Nanoengineering, UNC at Greensboro, 2907 E. Gate City Blvd, Greensboro, NC 27401, USA.
E-mail: j_wei@uncg.edu
[b] Savannah River National Laboratory (SRNL), Aiken, SC, 29808, USA.
E-mail: simona.murph@srnl.doe.gov
[c] University of Georgia (UGA), Athens, GA, 30602, USA

obstacle to precisely determining mercury species in natural aqueous environments.[10]

Efforts are underway to develop analytical strategies for the early and accurate detection of ultra-trace levels of mercury in environmental samples. This is crucial for timely remediation and controlling contamination sources to mitigate the adverse effects of mercury exposure.[11]

Various analytical techniques are currently in use for mercury detection. For example, atomic absorption spectroscopy (AAS) is employed for total mercury and methylmercury analysis in dried blood and fish samples.[17–20] Cold vapor atomic fluorescence spectrometry (CV-AFS) is employed for detecting mercury in environmental water samples.[21–23] Additional methods include cold vapor atomic absorption spectroscopy (CV-AAS),[24] inductively coupled plasma-mass spectrometry (ICP-MS),[25–27] anodic stripping voltammetry,[28,29] and X-ray fluorescence spectrometry (XFS).[30,31] Many of the aforementioned analytical methods allow for the analysis of numerous samples including multiple elements simultaneously. However, it is worth noting that most of these methods involve a multi-step process, including sample collection, laboratory pretreatment, and subsequent mercury level analysis.[32] This makes the procedures operationally complex, labor-intensive, time-consuming and costly.

Moving away from conventional, stationary, expensive, and skill-intensive instrument that necessitates complex sample preparation procedures, there is a high demand for a new generation of analytical techniques that are user-friendly, cost-effective, reliable, accurate, and portable for on-site deployment (Fig. 1).[33] A novel approach attracting attention in mercury sensing techniques involves the use of functional materials such as metal nanoparticles (NPs) and thin-film nanostructures.[34] The unique characteristics of metal NPs and thin-film nanostructures, such as size and shape variability, surface functionalization, and high surface area-to-volume ratio, have gained interest for their application in heavy metal detection, including mercury.[35] For example, surface-enhanced Raman spectroscopy (SERS) technique, in which the Raman scattering vibrations of molecules adsorbed to nanoscale metal surfaces are strongly enhanced, has emerged as a viable alternative to overcoming the limitations of conventional analytical methods, offering a more sensitive, cost-effective and non-destructive solution.

Although nanomaterial-based sensors possess high sensitivity, achieving selectivity for specific targets remains a for-

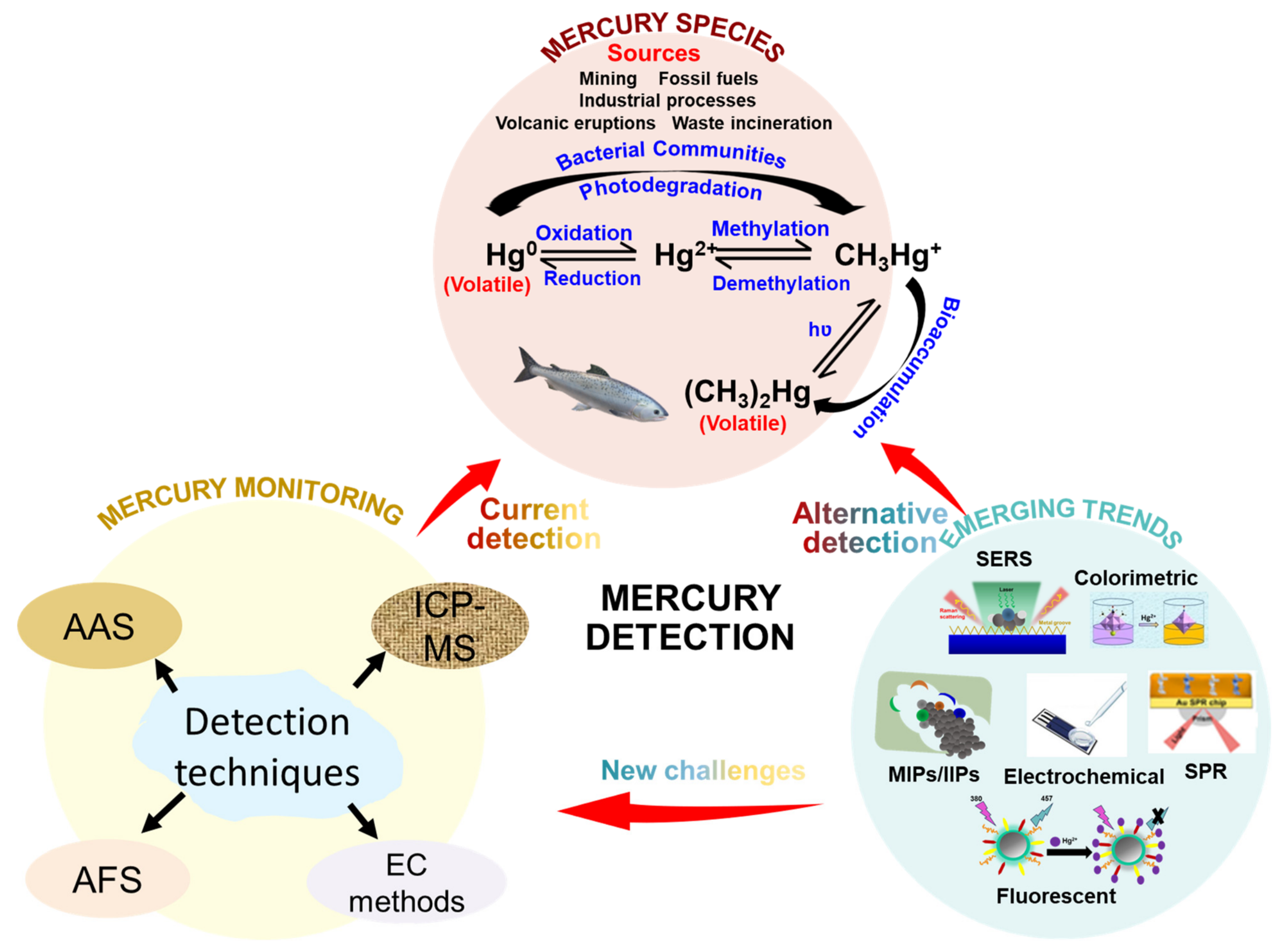

Fig. 1 Schematic diagram showing the major sources and forms of mercury contaminants and various conventional and emerging techniques for the detection of mercury species in environmental samples.

midable challenge. In addressing this issue, molecularly or ionically imprinted polymers (MIPs or IIPs) have surfaced as a promising technique for enhancing the selectivity of detection across various analytes.[36,37] Remarkably, MIPs/IIPs boast customizable features that support elevated affinity and selectivity toward designated target molecules. As a result, they play a pivotal role in mitigating the selectivity constraints observed in other chemosensor platforms.

In this review, we thoroughly examine the significant recent advancements in SERS and IIP-based mercury sensors, evaluating their potential as simplified alternatives to complex mercury detection methods. We begin by exploring various SERS sensor structures and configurations, with a specific focus on the strategic use of metal NPs and thin-film nanostructures for signal enhancement. These elements contribute to the development of robust SERS platforms, emphasizing the selection of molecular species as Raman reporters and capture molecules for mercury species.

Moving forward, we delve into the MIP- or IIP-based chemosensing approach, highlighting the strategies used for tailoring the properties of the polymer platform to ensure the selective capture of mercury. We encompass the approaches to enhancing sensitivity through the utilization of nanomaterials and complementary sensing strategies for precise mercury detection in environmental samples.

The review discusses the challenges associated with both SERS and MIP techniques, particularly in achieving sensitive and discerning mercury capture in environmental samples. The concluding remarks shed light on viable SERS and MIP/IIP platforms that could be successfully implemented in the realm of environmental protection while providing valuable insights into future research prospects of these technologies.

2. Environmental mercury species

Mercury typically manifests in three distinct states: elemental (Hg^0), ionic (Hg^{2+} and CH_3Hg^+), and molecular (phenylmercury and dimethylmercury $(CH_3)_2Hg$). Once released into the environment, it can easily transition between air, water, sediment, soil, plants, and animals. Notably, 80% of anthropogenic mercury emissions into the atmosphere result from industrial processes, with coal-burning power plants contributing 42% to this total.[38–40] These processes release elemental mercury into the air in the form of vapor or particles, which are dispersed by wind currents, eventually settling on land and water bodies. Rainfall can further wash down oxidized mercury ions, which may be absorbed by plants. Approximately 5% of elemental and aqueous mercury contamination in terrestrial environments stems from the discharge of industrial wastewater and the weathering of geologic reservoirs.[38] In soil and water, elemental mercury and mercury ions can undergo oxidation, transforming into mercury sulfide (HgS) or methylmercury in the presence of dissolved organic matter and microbes (Fig. 2). Methylmercury, known for its neurotoxic effects on the central nervous system, poses a significant risk. Seafood, particularly swordfish, tuna, and mackerel, serves as the primary entry point for methylmercury into the human body.[41]

3. SERS-based mercury chemosensors

The subsequent discussion delves into recent works in the field of SERS chemosensors designed for the detection of various mercury species. Raman spectroscopy is an analytical technique that allows chemical identification based on the inelastic scattering of incident light when impinged on molecules of interest. While only a small fraction of the photons are inelastically scattered, approximately 1 in 1 million, the response can be exploited with enhanced orders of magnitude in the presence of rough surfaces. Previous reports on SERS-active substrates from our group and others, comprised of colloidal metallic and/or metallic oxides, show 10^6–10^8 factor enhancements in Raman signals.[42–44] Therefore, SERS has emerged as a useful tool for the detection of traces of analytes of interest in various media. Strategic selection of the media used to probe analytes, *i.e.*, solution, gas, or solid, and the use of "hot-spot" bearing shape-selective metallic nanostructures, *i.e.* rods, triangles, stars, *etc.*, instead of spheres or targeted arrangement on support, *i.e.* distance, tip *vs.* side, oxidation state, *etc.*, can lead to different responses.[45–47] The origin of SERS signals arises from a combination of chemical contributions from analytes, Raman tags if used, and the electromagnetic excitation of surface plasmons. These surface plasmons are essentially electromagnetic fields at the surface of a metal–dielectric or semiconductor–dielectric interface.[48,49] Basically, by coupling the plasmon band of an irradiated nanometal (*i.e.*, gold, silver, copper, *etc.*) with the analyte'/molecules' electronic states, surface-enhanced Raman scattering effects are produced. This synergistic approach enhances the molecular scattering of light, leading to the amplification of Raman signals and heightened sensitivity. The appeal of SERS-based sensors lies in their ability to provide fingerprint identification of the analyte, ensuring a non-destructive and highly sensitive detection method. The deployment of nanomaterials in the construction of SERS substrates continues to provide impressive signal enhancement by a factor ranging from 10^6 to 10^{15}, depending on the strength of the electromagnetic field experienced by molecules at the surface of various plasmonic nanostructures.[50–52] Moreover, the use of nanomaterials in SERS not only enhances sensitivity but also facilitates the miniaturization of sensing platforms.[53] This, in turn, enables the implementation of these sensors for on-site or remote quantitative analysis of analytes, offering a practical solution for real-time monitoring of mercury levels in various environments.[54] The combination of enhanced sensitivity, non-destructive analysis or identification, and the ability to operate in on-site settings positions SERS-based sensors as promising tools for advancing our capabilities in detecting and monitoring heavy metals, including mercury-based analytes.[33]

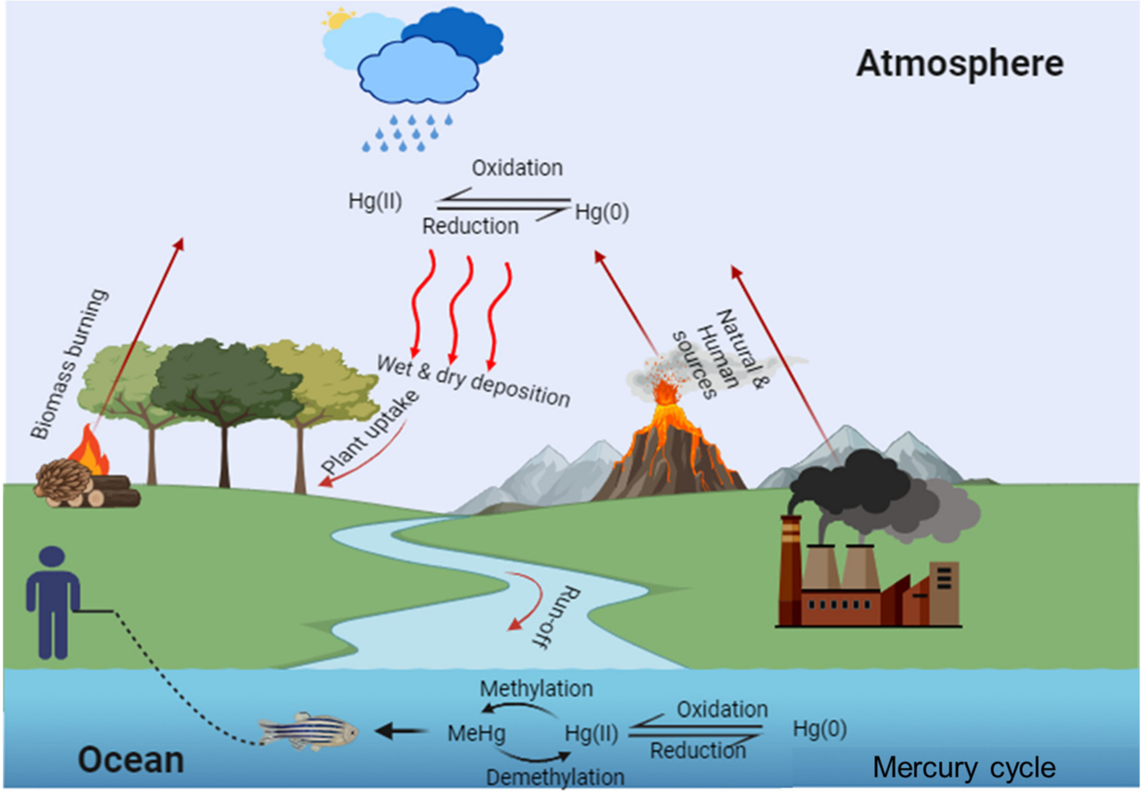

Fig. 2 Schematic view of the environmental mercury cycle.

3.1. SERS substrate configurations

Before the emergence of SERS, first-generation Raman spectroscopy was utilized in molecular identification, but it exhibited limitations such as weak signal intensity for sensitivity towards low-concentration analytes. In light of this, we pay greater attention to the ongoing progress of SERS in detection, specifically emphasizing the crucial aspects of sensor configurations and probes employed for mercury sensing. The development of chemosensors targeting mercury species through SERS can be broadly categorized into two configurations: solid SERS substrate (*e.g.*, in lab-on-a-chip sensing configuration) and colloidal SERS substrate (solution-based sensing configuration). Table 2 presents the comparison in terms of performance, cost, and fabrication methodologies.

The performance of solid and colloidal SERS substrate configurations demands careful consideration in selecting substrate materials and carefully designing the structures,[60] including NPs or nanostructures, Raman reporters, mercury-specific ligands, and support materials (illustrated in Fig. 3). These chosen materials must possess synergistic optical and chemical properties crucial for the effective functioning of any SERS sensor.[35]

Nanomaterials and nanostructures play a key role in generating localized electromagnetic field enhancements or "hot-spots", critical for amplifying SERS signals. Gold and silver nanomaterials are commonly selected due to their distinctive optical characteristics such as plasmonic enhancement, high Raman-scattering efficiency, chemical stability, facile functionalization, and ease of fabrication. These metals sig-

Table 2 Comparison of solid-SERS active substrates and colloidal SERS substrates

Configuration	Example	Fabrication methods	Reproducibility and sensitivity	Fabrication scalability	Cost	Functionalization	Ref.
Solid-SERS	Nanoslit arrays, rough metal surface, surface-immobilized NPs, nanopillars	Lithography, FIB milling, layer-by-layer assembly, PVD, 3D printing	Excellent reproducibility (5 nM to 0.1 pM)	High, with mature manufacturing processes	High	Excellent with various functionalization chemistries	55 and 56
Colloidal SERS	NPs, nanorods, nano cubes	Sol–gel hydrothermal, chemical reduction, laser ablation	Poor reproducibility (5 nM–1.11 fM)	Fair	Low	Excellent with various functionalization chemistries	57–59

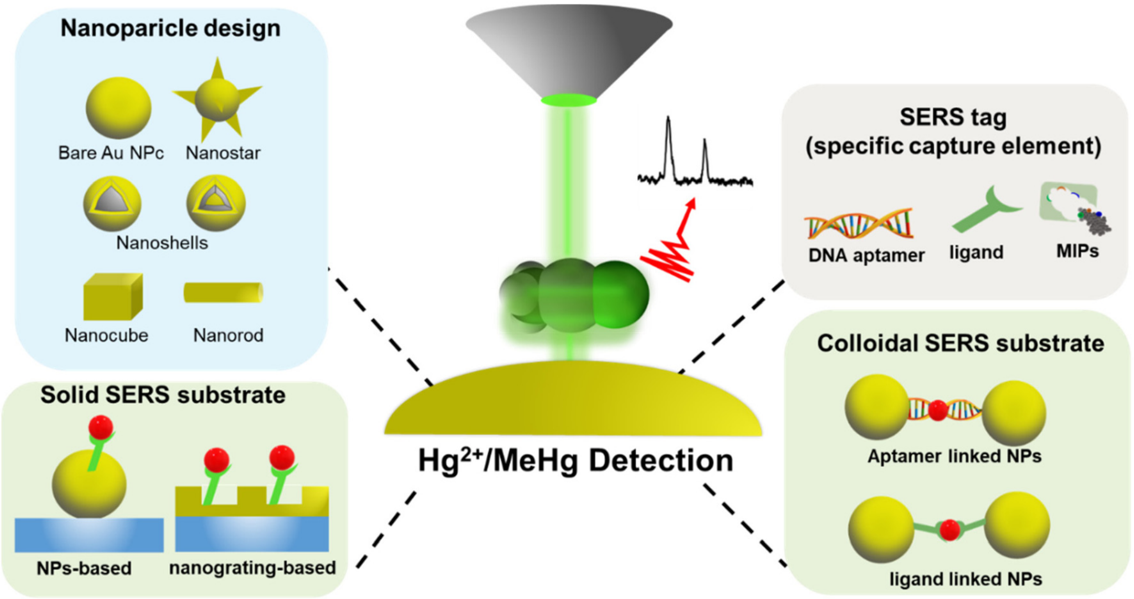

Fig. 3 Schematic illustration of the mercury-SERS chemosensor structure and configuration.

nificantly influence the sensitivity efficiency of SERS sensors.[61] Other non-noble metal materials used in SERS include carbon materials such as graphenes,[62] transition metal dichalcogenides such as MoS_2,[63,64] metal oxides,[65] metal–organic frameworks,[66] transition metal nitrides (MXenes) such as titanium nitride,[67] and conjugated polymers.[68] Raman reporters are also known to amplify Raman signals through chemical contribution while functioning as recognition molecules responsible for capturing targets.[69] Raman reporters are often self-assembled or covalently tethered to the NPs or nanostructures. In cases where recognition molecules lack the functionality to firmly attach to the nanostructure, a linker molecule like aminated alkane-thiol is used.[12] The organized and precise assembly of metal nanomaterials, analyte probes, and Raman tags is crucial for the sensitivity, selectivity, and overall reliability of SERS platforms.

3.1.1. Colloidal SERS substrates: solution-based SERS. Colloidal SERS platforms stand out as strong contenders for serving as effective SERS substrates in mercury detection. The dispersed colloidal material enhances the Raman signal of analytes, making it a powerful tool for this purpose. The colloidal SERS substrate configuration employs two basic strategies for detecting mercury species (Fig. 4).

The first strategy using colloidal substrates involves direct sensing, where the responsive SERS signal generation occurs when the analyte directly adsorbs onto the surface of the colloidal particles. The Raman signal is quenched or amplified based on whether the analyte is in contact with the substrate surface. To achieve this in a colloidal SERS system, the analyte must have sufficient surface affinity to penetrate a layer of stabilizing species and replace surfactants.[70] Analytes with functional groups enabling adsorption onto gold or silver nanostructures are more suitable for this strategy. To achieve optimal results, it is crucial to ensure a monolayer of analyte on the NPs. Furthermore, the NP junction and inter-particle distance should be controlled and evenly distributed, for instance, by employing dilute solutions and managing sample volume. Hence, the quantitation of the analyte is possible by correlating the Raman signal strength with the analyte concentration. However, this strategy is not suitable for detecting vibrationless atomic ion species such as Hg^{2+} due to their poor binding affinity to metallic surfaces.[71]

The second approach is indirect sensing by employing the SERS-tag strategy. Here, Raman reporters with distinctive Raman peaks are tethered onto the SERS substrate, acting as beacons for analyte detection. The SERS spectrum of the reporters provides characteristic spectral fingerprints that selectively indicate the presence or absence of chemical or physical interactions with the analytes.[72] This approach requires the analyte to have a significantly high affinity to the Raman reporter. The interaction causes a change in the geometric conformation or electronic redistribution of the reporter moieties, generating a unique Raman signal for quantifying the analyte.[73] An ideal Raman reporter should exhibit a distinctive and sensitive SERS signal response to enable better visibility of changes occurring in the presence of the analyte. These changes could be in the form of peak shifts, intensity fluctuation, appearance, or disappearance of the SERS peaks of the Raman reporter. It is also beneficial for the Raman reporter to have at least dual functionality to bind to the substrate and form a complex with the analyte target.

Given the challenges in directly detecting inorganic forms of mercury, in particular Hg^{2+} ions, and due to their small Raman scattering cross-section and lack of vibrational modes, the use of Raman reporters has proven to be beneficial in providing an indirect signal for quantifying the ion.[74] For

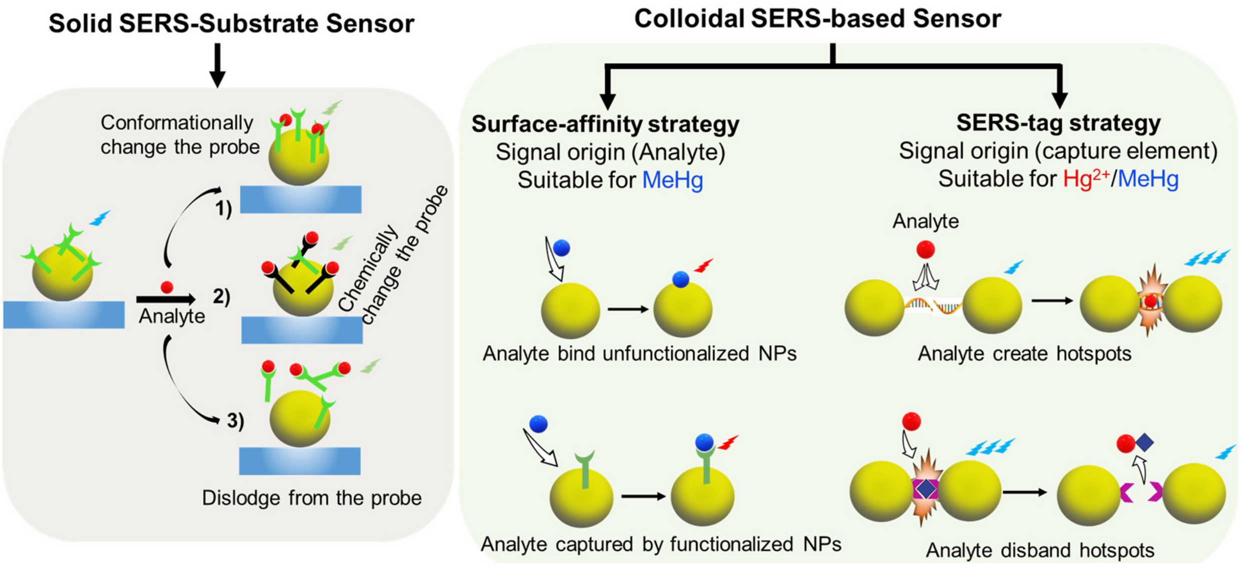

Fig. 4 Strategies and principles of indirect mercury detection with solid-SERS substrates and colloidal-SERS active substrates.

instance, Lea *et al.* developed a silver NP (AgNP)-based SERS platform, pioneering the use of a tethered rhenium carbonyl complex as a Raman reporter for Hg^{2+} detection.[75] In a recent study, magnetic Fe_3O_4@SiO_2@Au core/shell NPs modified with 4-mercaptopyrindine (4-MPY) served a dual role of a Raman reporter and a mercury-specific ligand. This strategic configuration was used as a SERS sensor for detecting Hg^{2+} in water and macrophage cells.[73] The recorded SERS signals of 4-MPY were employed for quantifying Hg^{2+}, demonstrating a linear increase in the SERS response with rising mercury concentration and a limit of detection (LOD) of 1 ppb (Fig. 5A). This platform exhibited high performance in terms of repeatability, selectivity, and long-term storage stability. Various other Raman reporters including methylene blue,[76] crown ether,[12] MPY,[77] 4,4′-dipyridyl (Dpy),[34] and DNA/oligonucleotide-conjugated dye tags such as cy3 [72] have been used to indirectly correlate the changes in the absolute SERS intensity of a Raman reporter for mercury detection.[78] Table 3 provides a summary of the different SERS sensor configurations and Raman reporters employed for Hg^{2+} detection.

In the pursuit of detecting and discriminating mercury species, Guerrini *et al.* developed a sensing platform consisting of a self-assembled monolayer of 4-MPY on a hybrid plasmonic material in the form of gold NPs anchored onto polystyrene microbeads.[82] This platform achieved simultaneous detection, quantitation, and discrimination of inorganic Hg^{2+} ions and organic mercury (CH_3Hg^+) species. The mechanism is based on the coordination of Hg^{2+} and CH_3Hg^+ to the nitrogen atom of the MPY ring. The chelation of Hg^{2+} occurs *via* multidentate N-bonding with MPY molecules, while methylmercury forms unidentate complexes with the pyridine moiety of MPY. The sensor demonstrated an LOD of 0.1 ppb and 1.5 ppb for mercury(II) ions and methylmercury, respectively. MPY offers significant advantages compared to other ligands, being bifunctional, allowing binding to the gold surface *via* its mercapto group and coordinating both CH_3Hg^+ and Hg^{2+} species differentially in the SERS signal *via* the nitrogen of the pyridine moiety. The coordination of metal ions to the pyridinic nitrogen atom induces a redistribution of electron density within the aromatic ring, reflected directly in the vibrational spectrum of the molecule.

In a more recent report, Chen, *et al.*, proposed a bimodal (colorimetric and SERS) detection strategy using a gold nanorod, modified by a stimuli-responsive *p*-amino-thiophenol (PATP) as signal readout to detect Hg^{2+} and CH_3Hg^+ in water, food and human hair (Fig. 5B).[79] The authors noted that Hg^{2+} is reduced with the assistance of PATP to form Hg^0, which is deposited onto the surface of the GNRs, leading to a hypsochromic shift of the longitudinal SPR band. Furthermore, CH_3Hg^+ triggered an end-to-end aggregation of GNRs due to its excellent coordination ability toward the $-NH_2$ group of PATP, inducing color changes from wine-red to blue, thus allowing visual detection with the naked-eyes. The "turn-on" SERS method and colorimetric assays based on the interaction between GNRs@PATP and mercury species provided an LOD of 3.2 fM for Hg^{2+} and 0.3 nM for CH_3Hg^+. A negligible cross-interference between Hg^{2+} and CH_3Hg^+ was recorded, further stressing the selectivity of the sensor scheme.

The colloidal SERS method, while sensitive to femtomolar levels of mercury species, faces stability issues due to signal fluctuations caused by dynamic colloid motion and auto-aggregation of NPs from external interferences such as pH, temperature, and salt concentration.[83] This can lead to false-positive signals and reproducibility problems. Non-specific interaction of most Raman reporters with other divalent metals, notably Pb^{2+}, As^{2+}, and Cd^{2+}, is another key drawback.[56] Some reported strategies to overcome cross-selectivity and reproducibility issues due to auto aggregation include masking colloidal NPs

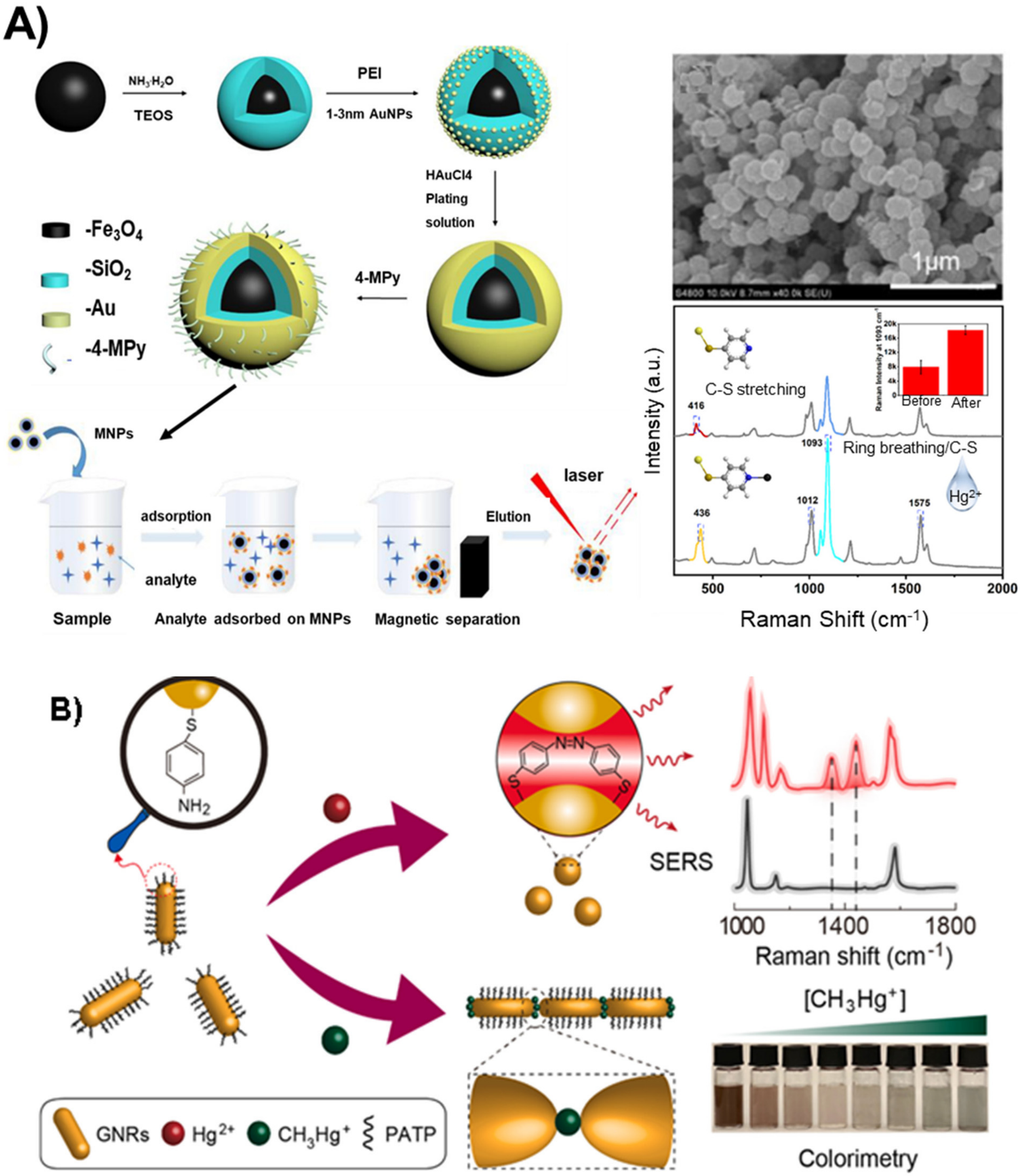

Fig. 5 Schematic of various colloidal SERS substrate platforms and fabrication techniques for mercury and methyl mercury measurements: (A) Synthetic route of $Fe_3O_4@SiO_2@Au/4$-MPy magnetic composite microspheres and the SERS detection of Hg(II) ions absorbed on $Fe_3O_4@SiO_2@Au/4$-Mpy. Reproduced with permission.[73] Copyright 2023, MDPI. (B) Bimodal (colorimetric and SERS) detection strategy to discriminate between mercury ions and methyl mercury using GNRs@PATP.[79] Copyright 2023, *Chem. Eng. J.* (C) Synthesis and sensing mechanism involved in the determination of Hg^{2+} in fish and water samples using Au@Ag NPs@R6G. Reproduced with permission.[80] Copyright 2021, Elsevier. (D) Synthesis and functionalization processes of AgNPs and their application for the SERS detection of Hg^{2+} using 4,4′-dipyridine as a probe. Reproduced with permission.[81] Copyright 2022, Journal of Applied Spectroscopy.

with reagents such as 2,6-pyridinedicarboxylic acid.[41,42,85] Notably, the use of DNA/oligonucleotides as probes provides a popular approach, offering some level of aggregation control and selectivity toward Hg^{2+} ions.[86] The high affinity of Hg^{2+} to thymidine is exploited to induce hybridization or conformational changes in DNAs tethered on the surface of metal

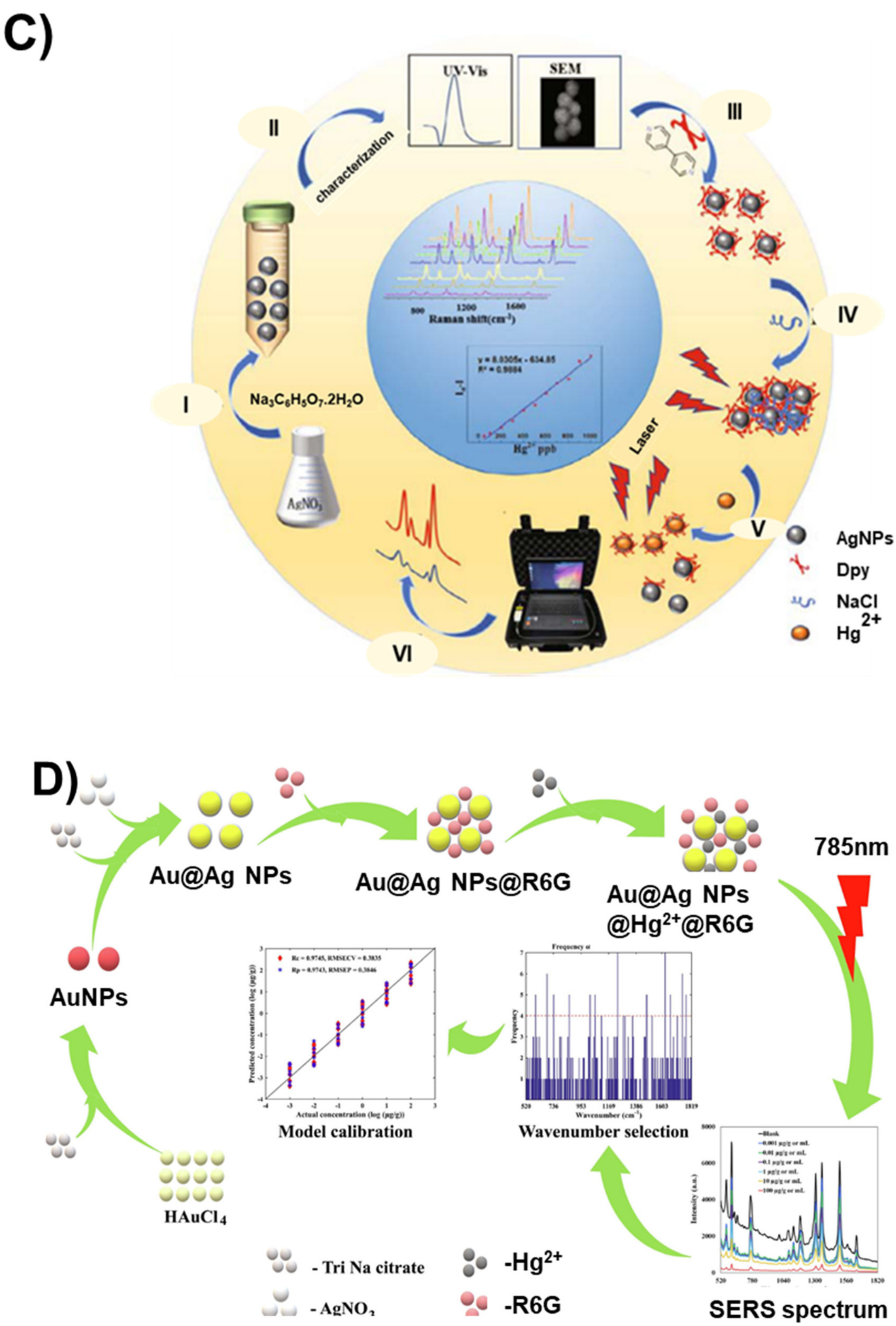
C)
UV-Vis
SEM
II
characterization
III
IV
I
Na3C6H5O7.2H2O
AgNO3
Raman shift(cm-1)
800
1200
1600
y = 8.0305x - 634.85
R² = 0.9884
Hg2+ ppb
Laser
V
VI
AgNPs
Dpy
NaCl
Hg2+
D)
Au@Ag NPs
Au@Ag NPs@R6G
Au@Ag NPs
@Hg2+@R6G
785nm
AuNPs
HAuCl4
Model calibration
Wavenumber selection
SERS spectrum
Rc = 0.9745, RMSECV = 0.3835
Rp = 0.9743, RMSEP = 0.3846
Predicted concentration (log (µg/g))
Actual concentration (log (µg/g))
Frequency
Wavenumber (cm-1)
Intensity (a.u.)
Blank
- Tri Na citrate
- AgNO3
-Hg2+
-R6G

Fig. 5 *(Contd)*.

Table 3 Summary of SERS biosensors and probes for Hg^{2+} detection

SERS biosensor design	Raman reporter	Probe–target interaction/sensing mechanism	Linear range	LOD	Ref.
Magnetic Fe_3O_4@SiO_2@Au core/shell NPs, functionalized with 4-MPY (colloidal SERS)	4-MPY, also to capture Hg^{2+} ion	Hg^{2+} causes changes in the electronic distribution of 4-MPY, resulting in spectral blue shift and Raman signal enhancement	10 ppm–1 ppb	1 ppb (4.99 nM)	73
AuNPs, functionalized with MBA (colloidal SERS)	4-Mercaptobenzoic acid (MBA)	Hg^{2+} complexes with –COOH group of MBA, leading to AuNP dimers, trimers, *etc.* and hot spots creation. Phenomena is not observed with CH_3Hg^+	1 ppb–10 ppt	5 ppt (0.025 nM)	84
DNA modified AuNPs (colloidal SERS)	4-Nitrothiophenol (4-NTP) as reporter	DNA selectively captures Hg^{2+} by forming T–Hg^{2+}–T complex	0.001–0.5 ng mL^{-1}	0.45 pg mL^{-1} (2.24 pM)	87
Core–shell Au@Ag NPs (colloidal SERS)	Rhodamine 6G (R6G) as signaling probe for Hg^{2+}	In the presence of Hg^{2+}, citrate ion of Au@Ag NPs induced complexation and become amalgam, causing desorption of R6G, thus a decrease in SERS signal intensity.	10^2–10^{-3} μg g^{-1}	0.001 μg mL^{-1} (4.99 nM)	80
Au film deposited on nanorod arrays etched on Si wafer, and functionalized with 4-MBA (solid-SERS)	4-Mercaptophenylboronic acid (4-MBA)	Hg^{2+} is trapped by 4-MBA through electrophilic substitution reactions resulting in geometric reconstruction of 4-MBA to 4-mercaptophenyl mercury chloride	10^{-5}–10^{-10} M	0.1 nM	104
Au nanostar@Ag satellite (AuNSt@AgSAT) sandwiched with BDT (colloidal SERS)	1,4-Benzenedithiol (BDT)	The presence of Hg^{2+} resulted in amalgamation of the AuNSt@AgSAT, which altered both its structural morphology and Raman enhancement properties	50–1000 ppb	0.1 ppb (0.5 nM)	105
Ag nanowires/glass transparent conductive film functionalized with L-cysteine (solid SERS)	L-Cystein	Hg^{2+} adsorption onto –COOH– of L-Cys causes a change in the ring-breathing of associated SERS bands of Ag NW-L-Cys	10^{-12}–10^{-7} M	1 nM	106
Capillary decorated with AuNPs, functionalized with 4-MPY (solid SERS)	4-MPY, also to provide anchoring sites for Hg^{2+}	Pyridine nitrogen of 4-MPY captures Hg^{2+}, changing 4-MPY orientation from flat to perpendicular, thus modifying SERS signal intensity ratio	0.1 μM–1 pM	0.2 pM	107
Au@Au core–shell NP modified with R6G Raman reporter and a thiolated single strand DNA probe immobilized on a lateral flow strip (solid SERS substrate)	R6G as Raman reporter and ssDNA as Raman probe	—	0.01 nM to 1 nM	0.3 pM	108

NPs, offering control of interparticle distance.[86] The strategy produces either a turn-on or turn-off SERS signal.

The turn-on mechanism in SERS signals using DNA oligos is based on thymidine–Hg^{2+}–thymidine (T–Hg^{2+}–T) coordination chemistry, generating plasmonic hotspots that enhance SERS signals of Raman reporters when colloidal particles aggregate. This strategy offers high selectivity and sensitivity due to the affinity of Hg^{2+} to thymidine and the strong electromagnetic field generated due to the plasmonic coupling of NP assemblies. For instance, Xu *et al.*, used Hg^{2+} to induce the aggregation of DNA-modified gold NPs (AuNPs) into chains.[87] They reported a remarkable SERS signal where the length of gold nanochains was directly proportional to the mercury ion concentrations over 0.001–0.5 ng mL^{-1} and the LOD in drinking water was as low as 0.45 pg mL^{-1}. Adopting a similar approach, a single-stranded DNA-modified gold nanorod (ssDNA-AuNR) undergoes hybridization with a partly complementary, fluorescently tagged DNA to form a double-stranded DNA-modified gold nanorod (dsDNS-AuNR) in the presence of Hg^{2+} ions.[88] An SERS detection method of Hg^{2+} *via* the nanorod side-by-side assemblies recorded a limit of detection of 0.001 ng mL^{-1} over a linear range of 0.01 ng mL^{-1} to 10 ng mL^{-1} in tissues and eggs of hens. Applying this strategy, the authors also detected methylmercury in egg whites. Liu *et al.* also utilized oligonucleotide-functionalized core/shell magnetic silica@Au NPs for SERS detection of Hg^{2+} ions based on a signal turn-on mechanism.[89] They recorded a distinct SERS intensity as the Hg^{2+} concentration increases in the linear range of 0.1–1000 nM and an LOD of 0.1 nM. Without necessarily undergoing any modification, the sensor effectively detects silver and enables the removal of both mercury and silver ions from the surrounding solutions by an external magnetic field.

The turn-off signal mechanism arises from the dispersion of NPs, caused by mercury ions displacing the Raman reporter from the NP surface. For instance, in a system utilizing aptamer-modified Au@Ag core–shell NPs with microfluidics for trace Hg^{2+} analysis *via* SERS, a Cy3 molecule as a Raman reporter attached at the 5′ end of a DNA aptamer exhibits significant signal reduction with the increase in Hg^{2+} ions.[72] This occurs due to the release of Cy3-labeled aptamer DNAs from the NP surface, forming stable T–Hg^{2+}–T-mediated hairpin structures. The sensor achieves an LOD of 10 pM.

Despite the widespread use of DNA oligos to enhance selectivity and control NP aggregation, their susceptibility to temperature, stability, and pH changes poses challenges.[90] To address these challenges, a strategy involving the use of electron-rich inorganic compounds such as 4,4′-dipyridyl (Dpy) is employed to induce colloidal dispersion. In this way, Du *et al.* designed a SERS chip specifically for detecting femtomolar concentrations of Hg^{2+}.[34] The chip utilized Au@Ag NPs that were modified with Dpy. In the structure of Dpy molecules, two pyridine rings are arranged symmetrically. The two electron-rich nitrogen atoms of Dpy bind to the silver shells of two Au@Ag NPs, inducing colloid aggregation. This aggregation creates a strong Raman hot spot effect, resulting in enhanced SERS readouts. In the presence of mercury, Dpy exhibits a strong affinity to mercury ions, leading to the formation of a Hg^{2+}-Dpy coordination complex. This coordination causes the exchange of Dpy from the surface of the NPs into the aqueous Hg^{2+} droplet. As a result, Au@Ag NPs become dispersed and the SERS signals are quenched. The chip demonstrates a rapid response to as low as 10 femtomolar (fM) Hg^{2+} within 4 minutes.

The detection and quantitation of mercury in traditional Chinese medicine preparation were achieved by using silver NPs (AgNPs) as the Raman substrate and Dpy as the signal probe (Fig. 5C).[81] In this methodology, Dpy was adsorbed onto the surface of AgNPs through an Ag–N bond. Subsequently, sodium chloride was introduced as a supplement to induce the aggregation of AgNPs, thereby enhancing its signal. Upon the presence of Hg^{2+}, Dpy forms a Dpy-Hg complex, which dissociates from the surface of the AgNPs, resulting in the dispersion of AgNPs and a subsequent reduction in their signal. The system demonstrated an LOD of 10 ng mL^{-1} within the linear range of 50–100 ng mL^{-1}.

Similarly, Hassan *et al.* utilized Rhodamine 6G (R6G) as a molecular probe in a core–shell Au@Ag NP-based SERS substrate for quantitative Hg^{2+} detection in fish and water samples (Fig. 5D).[80] In the presence of Hg^{2+}, R6G is displaced from the NP surface due to the formation of a mercury and citrate ion amalgam, resulting in a quenched Raman signal. The method exhibits an LOD of 0.001 μg mL^{-1} over a mercury concentration range of 10^{-3} to 10^{2} μg g^{-1}.

While these methods demonstrate satisfactory sensitivity and selectivity, achieving repeatability and stability remains a challenge.

3.1.2. Solid SERS-active substrates.

A solid SERS substrate consists of nanostructures (such as nano gratings and nanopillars) or nanomaterials (including NPs, quantum dots, and magnetic NPs) that are either directly fabricated or independently immobilized on a flat solid support. This support imparts a balance of flexibility and mechanical robustness, and materials such as glass, metals, polycarbonates, and other polymers are commonly used.[91,92] Glass supports offer good mechanical strength, but they tend to be fragile. Furthermore, supports like polymers possess necessary multifunctional characteristics such as mechanical strength and flexibility, in addition to cost-effectiveness, optical transparency, and metal-loading capability, which make them suitable for hosting and enriching metal nanostructures while providing tunable sensing outcomes.[75,93] The supports do not contribute typically to the SERS effect as they do not absorb or scatter light.

Active SERS nanomaterials can be introduced to a support through methods like direct drop casting, support engineering *via* etching or functionalization, or by growing nanomaterials on the support during the synthesis process to form a composite material.[94] Higher-order assemblies can also be achieved *via* these techniques or decorating the support surface with SERS-active NPs, or modifying the support with materials such as graphenes.[95]

Solid-SERS substrates offer several notable advantages including convenient handling and transport, enduring stability over time, enhanced reproducibility, and the potential for on-site applications. However, one of the primary challenges encountered in SERS techniques for mercury analysis pertains to the uniformity of the substrate, a factor that can significantly impact the reproducibility and reliability of sensing results. The consistency of SERS enhancement across the entire surface relies on uniform substrates, thereby ensuring more accurate and reliable measurements. In contrast, non-uniform substrates may yield inconsistent SERS enhancement, leading to unpredictable results and complicating the differentiation between analyte peaks and substrate-induced signals. Recent advancements addressing these challenges involve employing 3D printing techniques with femtosecond lasers, providing precise control over the size and distance between nanostructures.[55,86,96] This technology has shown promise in creating substrates with improved uniformity and enhanced sensitivity for mercury analysis.

Efficiency in SERS measurements is also influenced by the incident laser wavelength, impacting both penetration depth and light scattering efficiency.[97,98] In principle, the choice of material for SERS substrates, such as gold or silver, determines the optimal laser wavelength for the best Raman signal enhancement in terms of intensity and spatial resolution. For instance, a 785 nm laser is most effective with gold NPs, while a 532 nm laser performs better with silver nanoparticles.[99–101] A 630 nm laser can accommodate a mixture of both metals to leverage their respective enhancements.[102,103] With the expansion of SERS platforms to include non-noble metallic materials such as titanium nitrides, it becomes increasingly necessary to conduct SERS measurements at various laser wavelengths to determine the optimal wavelength for the specific material employed.

Another obstacle confronting SERS systems pertains to their selectivity. The platforms are susceptible to interferences owing to the restricted availability of mercury-specific probes and the diminished selectivity exhibited by the currently accessible probes. In studies aimed at detecting mercury species in environmental samples, gold and silver NPs have been favored for decorating support surfaces due to their excellent plasmonic and light scattering properties, as well as their ability to conjugate recognition ligands or directly bind with targets for improving selectivity.[75]

Another study illustrated the detection and quantitation of Hg^{2+} ions in water samples containing Pb(II) and Cd(II) interferents, achieving an LOD of 0.51 pM.[12] This was accomplished using a SERS sensor composed of gold nanostructures deposited on a gold support substrate. The surface of the substrate was functionalized with a crown ether derivative (from aminodibenzo-18-crown-6 coupled with mercaptopropionic acid, serving as a recognition molecule for Hg^{2+} ions). The capillary designed sensor exhibited a linear detection range of 1×10^{-11} M to 1×10^{-6} M Hg^{2+} ions.

Li *et al.* designed a methodology that integrates a self-driven microfluidic surface-enhanced Raman scattering (SERS) detection chip on a silicon support.[96] This was achieved using a femtosecond laser direct 3D writing (FLDW) technology, which enabled the detection and quantification of Hg^{2+} in water samples. The platform consisted of microchannels fabricated on silicon using a laser beam. Nanostructures were then created by FLDW at the junction of the microchannels, followed by the deposition of an Ag film, which served as the active SERS detection sites. Rhodamine 6G (R6G) was employed as the Raman probe molecule. Quantitative analysis of Hg^{2+} was achieved by separately injecting the Hg^{2+} sample and the probe molecule from two different inlets and collecting the SERS signal at the detection site. The authors determined that the designed platform could detect and quantify Hg^{2+} within a linear range of 10^{-3} to 10^{-9} M, with an LOD of 1 nM. A detailed summary of recent representative SERS sensors for mercury species detection is provided in Table 3.

3.1.3. Mechanisms of solid SERS for Hg^{2+} detection.

There are three prominent proposed mechanisms involved in detecting Hg^{2+} in a solid SERS substrate.

Mechanism 1: the first mechanism involves the alteration of the conformation or orientation of the probe immobilized on a solid support by the analyte. The change in the structure of the probe results in a unique Raman signal that corresponds to the presence of mercury. For example, Lu *et al.*, reported a label-free SERS sensor based on the formation of T–Hg^{2+}–T pairs and the corresponding effect on the orientation of DNA on the Au shell surface (Fig. 6A).[109] The DNA aptamer immobilized on the surface of SiO_2@Au core/shell NPs consisted of two segments, namely, the segment which has the consecutive thymines (T) serving as the Hg^{2+} recognition elements, and the segment which contains the guanine (G) and adenine (A) bases working as the signal reporter. The interaction of Hg^{2+} ions with the thymines between the adjacent single-stranded DNA (ssDNA) causes the DNA molecule to adopt a vertical orientation, resulting in an increase in the Raman intensity, as the concentration of Hg^{2+} increased. This allowed measurement of trace amounts of Hg^{2+} in aqueous solutions within a wide concentration range (from 1×10^{-8} to 1×10^{-3} M, LOD = 10^{-8} M). In a recent study, AuNPs were used to develop a label-free solid-SERS substrate chemosensor for the detection of Hg^{2+} and Ag^{+} ions in breast cancer cells (Fig. 6B).[110] The sensor was engineered by using a glass nanofiber support covered by the deposition of polystyrene-*b*-poly(4-vinyl pyridine) (PS-P4VP) diblock copolymers, which was further decorated by a layer of AuNPs that have been previously functionalized with a recognition molecule 4-MPY. The authors reported the intensity of the representative Raman bands to be increasing with the increase in the concentration of Hg^{2+} and Ag^{+} from 5 nM to 500 nM. The spectral changes were attributed to the effect of the 4-MPY molecular orientation (from flatter to more perpendicular with respect to the metal surface) arising from the coordination between the nitrogen on 4-MPY and the metal ions. The sensor achieved LOD values of 5 nM and 100 nM for Hg^{2+} and Ag^{+} respectively. Although the sensor showed selectivity in the presence of potentially interfering ions such as Al^{3+}, Cu^{2+}, Pb^{2+}, Co^{2+}, Ni^{2+}, Ca^{2+}, and Fe^{3+}, it could be challenging to detect Hg^{2+} ions in a sample containing Ag^{+} as an interferent due to the high affinity of 4-MPY ligands to Ag^{+}.

Mechanism 2: the second mechanism involves leveraging the chemical modification of the probe or Raman reporter induced by mercury. In this process, a chemical reaction occurs between mercury and the probe or Raman tag, resulting in the creation of a completely new substance on the surface of the Raman substrate. This transformation induces a modification in the original Raman spectra of the probe or Raman tag. For instance, Zhao *et al.*, reported ordered Au nanorod arrays (Au NRAs) modified with 4-mercaptophenylboronic acid (4-MBA) as multifunctional SERS reporters to detect Hg^{2+} in natural water (Fig. 6C).[104] Aqueous Hg^{2+} was efficiently trapped by 4-MBA *via* electrophilic substitution reactions, and precisely appraise its concentration based on the collective spectral changes of reporters including peak disappearance, emergence, and Raman shift. Based on this, the optical nanoprobe shows an ultrahigh detection sensitivity of 0.1 nM for Hg^{2+} and was able to identify different chemical forms of mercury based on their different chemical interaction with the 4-MBA probe. Another work, recorded the detection of Hg^{2+} *via* the galvanic replacement reaction (GRR) of Hg^{2+} on the silver nanorod surface using Victoria blue B as a molecular probe (Fig. 6D).[111] Upon addition of Hg^{2+}, the GRR occurred between AgNR and Hg^{2+} to form a larger size core–shell composite NP, $Ag_{core}/Hg_2Cl_{2shell}$, with low SERS activity that causes SERS signal quenching. Therefore, with the increase in the Hg^{2+} concentration, the SERS intensity decreased linearly in the range of 1.25–125 nmol L^{-1}, with a detection limit of 0.2 nM.

Recently, Guselnikova *et al.* have used gold gratings by employing their ability to excite a surface plasmon polariton (Fig. 6E).[112] They designed a competitive SERS chemosensor platform consisting of a recognition layer formed from a sunlight-induced thiolyne reaction of 4-ethynylphenyl groups with a mercaptosuccinic acid-based specific recognition layer in the presence of photocatalyst eosin Y. The sensor detected and quantified Hg^{2+} ions as low as 0.027 μg L^{-1}. The utilization of periodic metal grating produces a substantial surface area with an enhanced electric field uniformly distributed across the entire active surface of the sample. Such substrate is characterized by its simplicity in preparation, cost-effectiveness, and heightened sensitivity.

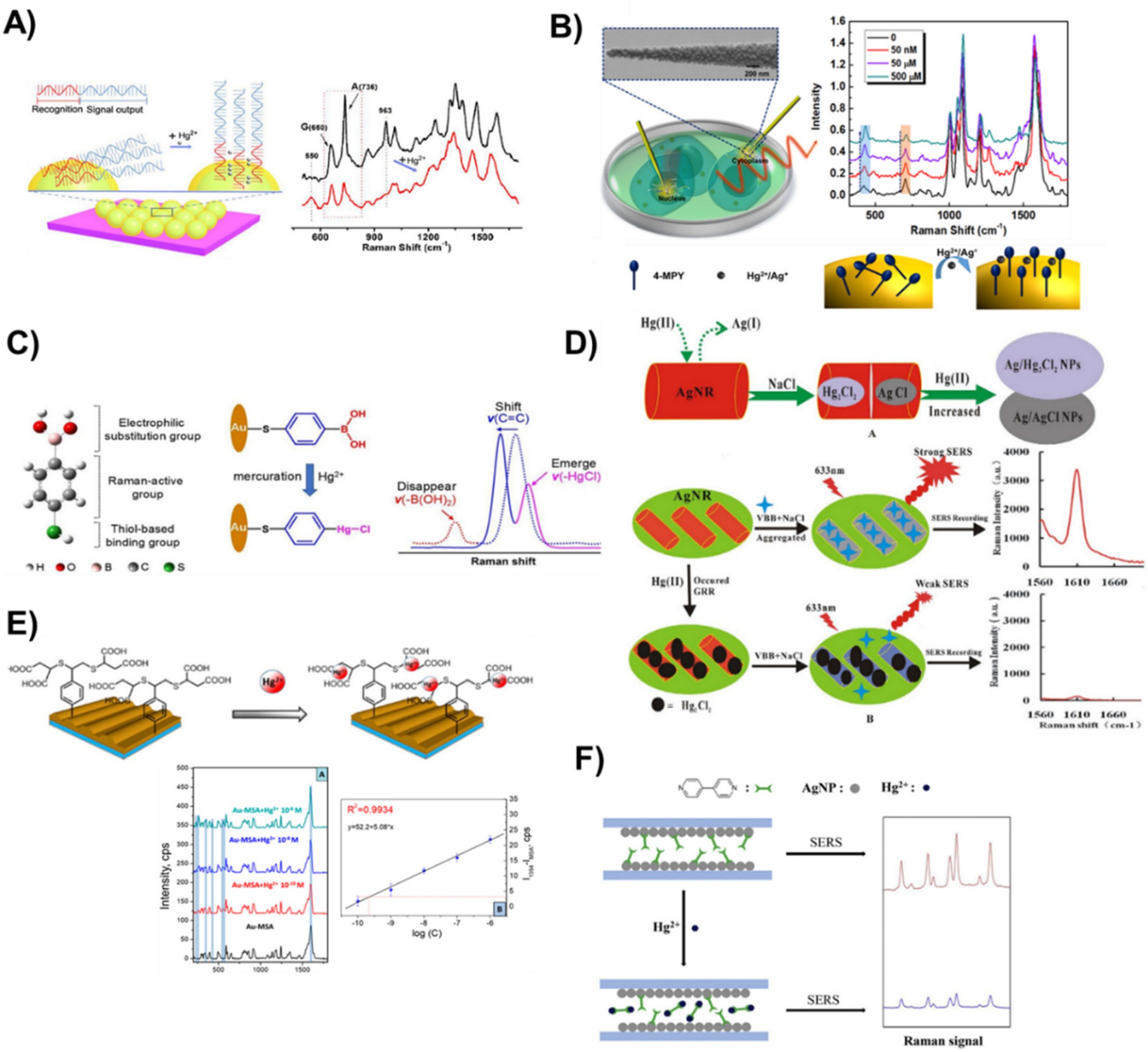

Fig. 6 Representation of various solid-SERS active substrate chemosensor designs, fabrication processes, and quantification techniques to detect mercury species. (A) Label-free SERS method for Hg^{2+} detection based on structure-change and orientation-switching ssDNA. Alongside is the typical SERS response of DNA aptamer-modified SiO_2@Au NP-based substrates in the absence (top spectrum) and presence (bottom spectrum) of Hg^{2+} ions. Reproduced with permission.[109] Copyright 2018, Elsevier. (B) A simultaneous quantification technique for Hg^{2+} and Ag^+ in cancer cells based on glass nanofibers decorated with AuNPs that are functionalized with 4-Mpy. Reproduced with permission.[110] Copyright 2021, American Chemical Society. (C) Schematic illustration of 4-MBA-based optical nanoprobes for accurate identification of Hg^{2+} based on mercuration-ruled electrophilic substitution to specifically anchor Hg^{2+} onto the probe *via* a chemical change. The spectral changes involve disappearance, emergence, and shift of vibrational peaks. Reproduced with permission.[104] Copyright 2020, Elsevier. (D) Illustrative steps for the detection of Hg^{2+}@Ag nanorods *via* galvanic replacement reaction using SERS. Reproduced with permission.[111] Copyright 2016, Nature Publishing Group. (E) Hg^{2+} ion capture *via* gold grating with mercaptosuccinic acid. Reproduced with permission.[112] Copyright 2019, Multidisciplinary Digital Publishing Institute. (F) Mechanism of detection of a solid-SERS sensor for quantifying Hg^{2+} *via* competitive ligand exchange in a capillary decorated with AgNPs that are coated with Dpy ligands. Reproduced with permission.[113] Copyright 2020, Elsevier. Copyright 2018, Elsevier.

Mechanism 3: the third mechanism for detecting Hg^{2+} entails a probe or ligand exchange between the SERS substrate and the mercury species. In this process, the probe's strong affinity for mercury leads to the formation of a probe-Hg complex, prompting the displacement of the complex from the substrate's surface. For example, Zhao *et al.* designed a quantitative SERS chemosensor based on a ligand exchange approach to detect Hg^{2+} ions in drinking water (Fig. 6F).[113] The chemosensor was designed as follows: (I) AgNPs were deposited on the inner walls of a glass capillary, previously functionalized with (3-aminopropyl)trimethoxysilane (APTMS); (II) the particles were conjugated with a 4,4′-Dpy ligand acting as a Raman tag and to capture Hg^{2+}. The interaction of the Hg^{2+} ions with Dpy causes the Dpy-Hg^{2+} complex to detach from the AgNPs. The detachment of the Raman tag produces relatively weak SERS readouts. The sensor was able to quantitatively measure the concentration of Hg^{2+} ions, and there was a proportional relationship between the Hg^{2+} ion concentration and the Raman peak response while achieving an LOD of 0.1 ppb (4.99 nM). The sensor shows practical applications by detecting Hg^{2+} spiked in environmental water samples and the recoveries were in the range of 96.10–102.06%.

The main challenge in the ligand exchange approach is the poor selectivity of probes. Other divalent metal ions present as impurities can also complex with ligands like Dpy, resulting in non-specific interactions. As a result, the concentration of Hg^{2+} in the ligand exchange analysis of environmental samples may be overstated and should be a source for further investigations.

3.1.4. Hybrid substrates of solid SERS for enhanced precision in Hg^{2+} ion detection. Solid-SERS substrates merged with colloidal or electrochemical approaches are shown to provide enhanced precision in Hg^{2+} detection. In the study by Feng *et al.*, a tetrahedral DNA structure was utilized in constructing a solid-colloidal hybrid substrate sensor that is superior in terms of selectivity, sensitivity, and stability over sensing approaches employing either colloidal or solid SERS substrates alone.[86] The hybrid SERS substrate was composed of satellite AuNPs tethered by tetrahedral DNA structures to a core AuNP supported on indium tin oxide (ITO). One edge of the tetrahedron featured single-stranded DNA containing an Hg^{2+} aptamer. Upon binding to the target Hg^{2+}, the Hg^{2+} aptamer underwent a structural transformation to a hairpin configuration due to the formation of the T–Hg^{2+}–T bond. This transformation induced the tetrahedra to shift from a relaxed state to a taut state. Consequently, the alteration in the tetrahedral structure brought the satellite AuNP closer to the core AuNP, generating robust SERS intensity owing to the surface plasmon coupling effect. A significant amplification in the SERS intensity was observed with the increase in the concentration of Hg^{2+} at the single-particle level. The lowest detection limit for Hg^{2+} was determined to be 0.36 nM.

In a recent study, Zheng *et al.* have unveiled a novel optical sensor featuring voltage enrichment, elevating the precision and sensitivity of Hg^{2+} ion detection.[56] As shown in Fig. 7, their research utilized nanoporous gold (NPG) modified with a cy5-labelled aptamer. The hybrid sensor leverages the coordination chemistry of thymine–Hg^{2+}–thymine interaction, coupled with an applied voltage that strategically propels mercury ions toward the NPG film. With a detection limit of 0.1 pM, the optical sensor demonstrated exceptional performance in aqueous solutions containing a diverse array of 13 metal ions. Notably, the method maintains reproducibility and stability, underlining its robustness for practical applications.

4. Mercury-based IIPs

IIPs have attracted considerable attention as a highly promising solution for the selective detection of heavy metals, such as mercury.[114] As synthetic materials, IIPs are designed to recognize and bind specific target ions with high affinity and selectivity.[115] They are easy to produce, exhibit impressive storage endurance without performance degradation, remain stable across wide temperature ranges, and maintain reliable imprint memory for over 100 cycles with little performance loss.[116,117]

The principle underlying IIPs is rooted in ionic recognition.[118] These polymers are prepared by polymerizing functional monomers with template ions, which are subsequently removed to leave behind a cavity that is complementary in shape, size, and chemical functionality to the template ion. The resulting IIPs can selectively bind to the template ion and demonstrate high affinity and selectivity towards it.

Considering the various forms of mercury (elemental Hg^0, ionic Hg^{2+} and CH_3Hg^+) and molecular states ($(CH_3)_2Hg$), the selection of a template governs target recognition and detection methods. In particular, the use of molecules such as dimethyl mercury ($(CH_3)_2Hg$) as the template during imprinting characterizes the approach as molecular imprinting polymers (MIPs). Conversely, the nomenclature IIPs denote the practice of employing ions, such as Hg^{2+}, to facilitate polymer imprinting.

4.1. Synthesis of IIPs

The synthesis of IIPs requires a functional monomer or polymerizable ligand, a crosslinker, and a polymerization initiator. Typically, a template ion is added before polymerization to model the target ion and create cavities intended for the selective recognition and binding of the target ion. For instance, to develop IIPs that selectively target mercury, the template molecules are usually small molecules containing a mercury ion, such as $HgCl_2$ or $Hg(NO_3)_2$. Fig. 8 illustrates the three general synthetic steps for IIPs, which are as follows: (a) the pre-polymerization step where functional monomers interact with the template ions in a solvent, (b) copolymerization of cross-linkers with the functional monomers, and (c) removal of the template from the imprinted polymers using an acid or a chelating agent.

This process is typically followed by grinding and sieving to achieve the desired particle size. These steps are common to various methods employed for synthesizing IIPs, including bulk, radical, sol–gel, and emulsion polymerization processes.[119–121] Among these methods, bulk polymerization is the most common synthetic approach for IIPs.[122] It is a one-step process that is easy to carry out and offers the advantage of controlling the amount and structure of the coordination compound embedded in the polymer's structure. However, it suffers from drawbacks such as low rebinding capacity, slow mass transfer, and incomplete removal of the template.[119,123] These limitations arise from the restricted accessibility of the binding sites within the rigid polymeric mixture. As a result, more attention is shifting towards surface imprinting techniques.

In the surface imprinting method, a thin layer of functional monomers is immobilized on solid supports, such as silica or glass beads.[123] Subsequently, the template ion is added to the functionalized surface, followed by polymerization and template removal. The resulting polymer layer contains imprinted

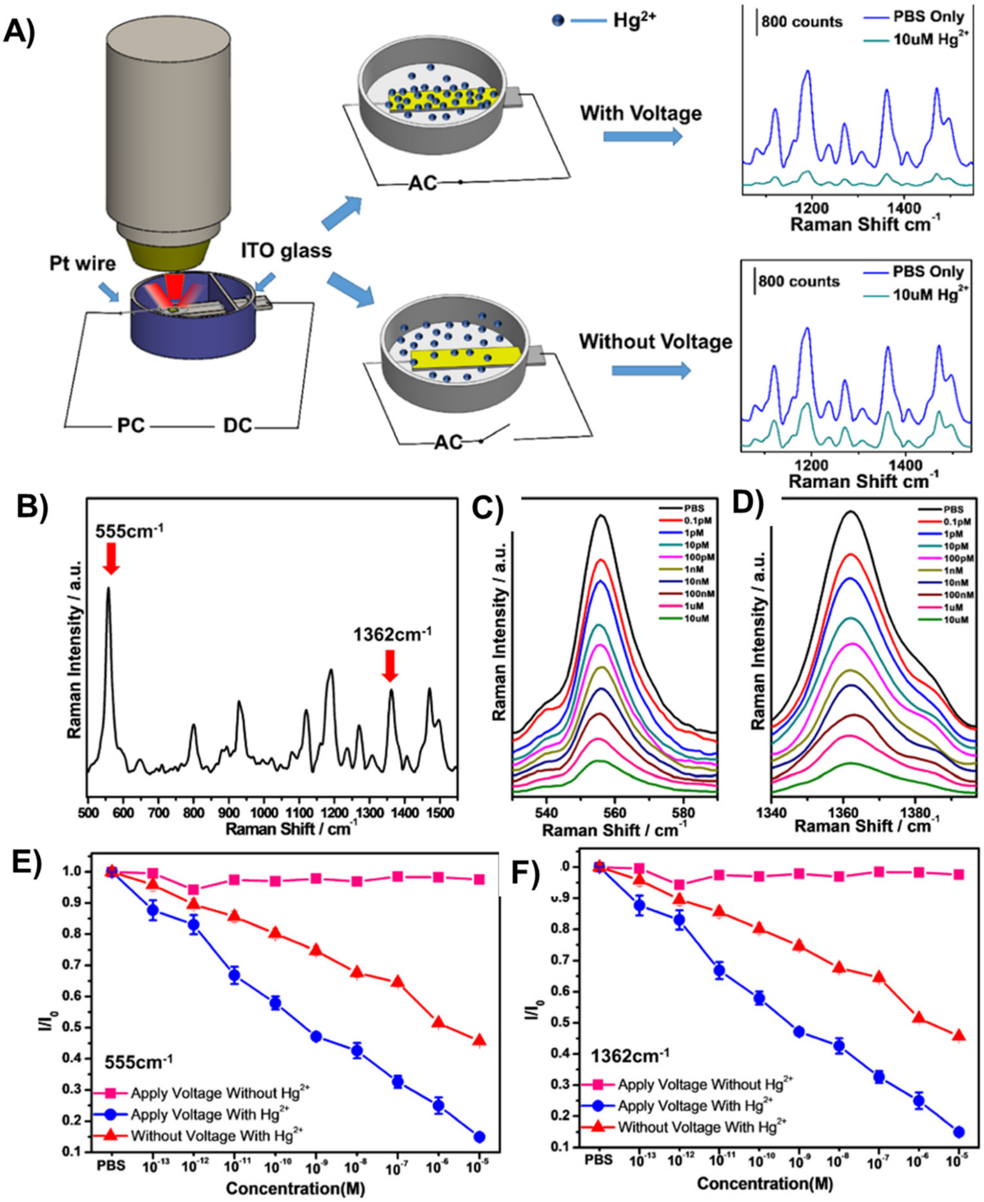

Fig. 7 (A) An NPG/aptamer sensor for Hg^{2+} detection based on voltage enrichment. (B) SERS spectrum of Apt15-modified NPG films and characteristic Raman peaks from Cy5 tags. (C & D) Characteristic peaks of Cy5 at 555 and 1362 cm^{-1} with different concentrations of Hg^{2+}. The SERS intensity of Cy5 reduces with the increase in Hg^{2+} concentration. (E & F) Normalized SERS intensity variation (I/I_0) of bands at 555 and 1362 cm^{-1} as a function of Hg^{2+} concentration in PBS. I_0 is the SERS intensity of Cy5 from the sensor in PBS only. Sensors with an applied voltage in the solution without Hg^{2+} (square); sensor without an applied voltage in the solution with different Hg^{2+} concentrations (triangle); sensor with an applied voltage in the solution with different Hg^{2+} concentrations (circle). Reproduced with permission.[56] Copyright 2019, American Chemical Society.

sites that are complementary to the template molecules/ions and are located on the surface of the substrate. This arrangement enables easy removal and rebinding of the template, thereby overcoming the drawbacks associated with the traditional bulk polymerization method.

4.2. Tailoring IIP properties for Hg detection

The properties and performance of IIPs for mercury detection depend on various factors including synthesis methods, nature of the target analyte, type of functional monomers employed, crosslinker, porogen, initiator, and polymerization conditions. These conditions influence the number of imprinted sites and the accessibility of the analyte to those sites.[119,124] The selectivity and sensitivity of the IIPs can be improved by optimizing these factors.

4.2.1. Choice of monomers and imprinting process. The selection of functional monomers is crucial for the development of IIPs for mercury detection, as the binding affinity and selectivity of the polymer rely on the chemical structure and functional groups of monomers. A critical requirement in

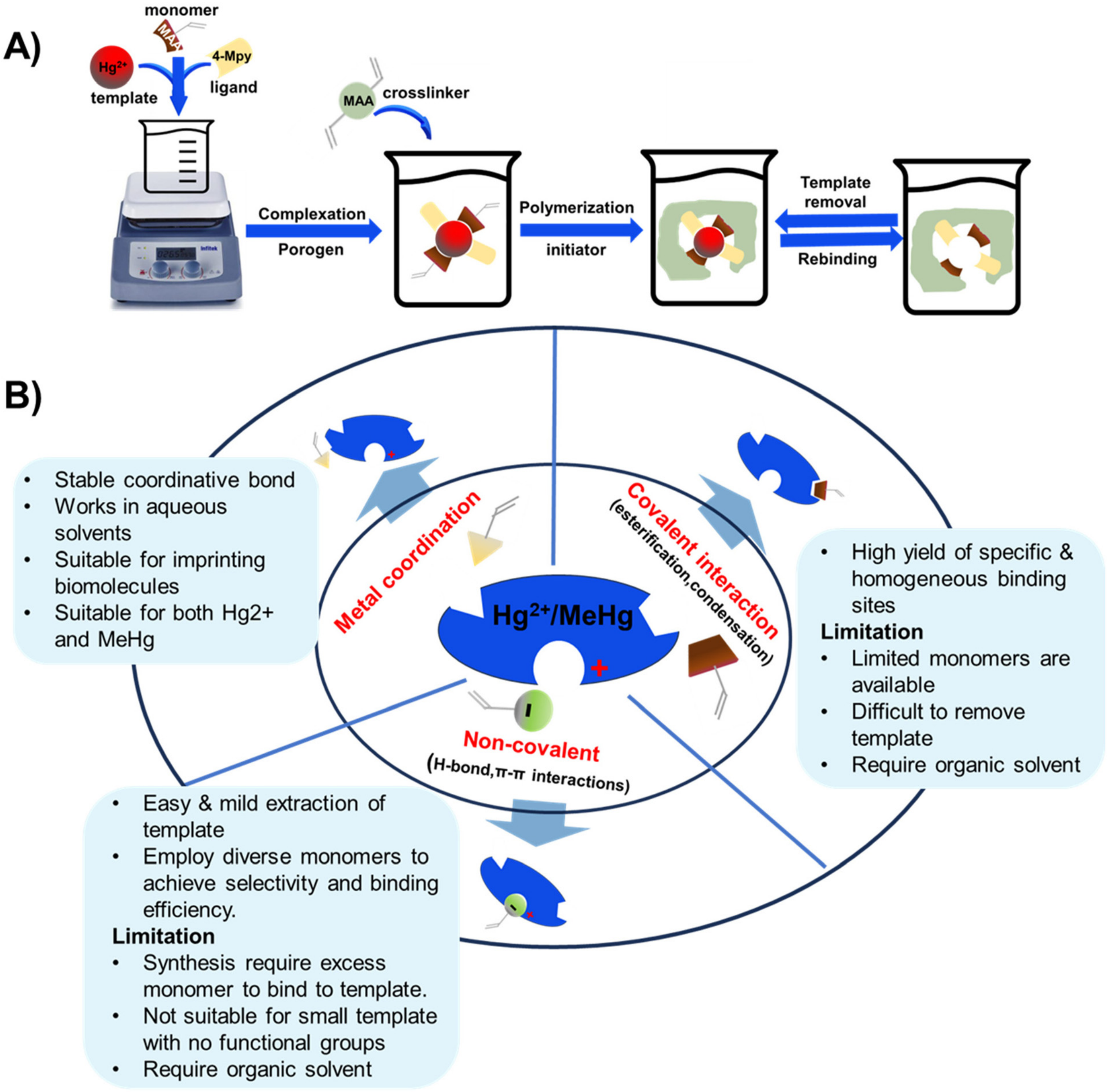

Fig. 8 Schematic showing (A) IIP synthesis and (B) various interactions of the template with functional monomers.

choosing the appropriate monomer is the presence of polymerizable functional groups such as vinyl, along with other functional groups such as thiols and carbonyls capable of interacting with the template. It is essential that these functional groups, apart from the polymerizable ones, do not interfere with or inhibit polymerization. Additionally, the monomer must remain stable throughout the polymerization process.

Commonly employed polymerizable commercial functional monomers containing nitrogen, sulfur, or oxygen atoms, such as acrylic acid, acrylamide, methacrylic acid, and 4-vinylpyridine, are used for the detection of Hg^{2+} and other heavy metals such as Pb(II) and Cd(II).[125–127] The suitability of these ionic templates arises from their distinct properties including solubility under imprinting conditions, strong and stable interaction with functional monomers, rigid conformation that fits the cavity of the polymer without altering its conformation, and ease of separation from and enrichment into the polymer matrix.[128]

The choice of the functional monomer dictates the nature of interactions between the functional monomers and templates during the pre-polymerization step. These interactions can be categorized into covalent, non-covalent, and coordination complex interactions (Fig. 8). Monomers interact with molecular mercury species such as dimethyl mercury through covalent or non-covalent interactions to form molecularly imprinted polymers (MIPs). Conversely, monomers can associate with mercury ions such as Hg^{2+} and $MeHg^{+}$ through coordination chemistry to form ion-imprinted polymers (IIPs).

Typically, monomers and ligands utilize heteroatoms (such as oxygen, nitrogen, or sulfur) to donate electrons to the unfilled orbitals of the outer sphere of the metal ions, thereby forming complexes.[3]

The covalent imprinting approach in molecular imprinting utilizes reversible covalent bonds such as reversible esterification or condensation reactions between the functional monomer and the template.[124] To achieve covalent interactions of analytes on IIPs/MIPs, the functional monomers and crosslinkers used in the synthesis of the IIP/MIP should facilitate chemical interactions with the template. The functional monomers need to possess chemical groups such as thiol, amino, or carboxyl groups, capable of reacting with the template species. Additionally, synthesis conditions such as polymerization temperature and time can be optimized to promote covalent interactions. For instance, higher temperatures and longer polymerization times can increase the degree of cross-linking and promote the formation of stronger chemical bonds between the IIP/MIP and the analyte.[129]

While this approach offers the benefits of producing specific and homogeneous binding sites, it suffers from the limited availability of monomers with the required functional groups such as alcohols (diols), aldehydes, ketones, amines, and carboxylic acids, which can participate in reversible covalent bonding.[130] This constraint restricts the applicability of the covalent imprinting approach to a narrower range of templates. Additionally, the removal of the template molecule is challenging, often requiring aggressive methods that utilize inorganic acids, which can damage the polymer matrix and alter the binding site's selectivity, reducing its effectiveness. As a result, the covalent imprinting approach is less attractive in practice.[131]

In comparing different eluents such as HCl, HCl + 5% thiourea, and HNO_3 for mercury removal from IIPs, HNO_3 is found to provide the best performance with over 99% recovery of mercury.[25,132] However, other reports indicate that HCl + thiourea offers enhanced performance and elution speed due to the complexing abilities of thiourea with mercury.[133]

The non-covalent interactions such as hydrogen bonding, π–π interactions, and hydrophobic interactions are more frequently employed in molecular imprinting due to their broader range of options for creating specific and selective binding sites without the drawbacks associated with covalent interactions. These interactions enable weak binding between the imprint molecule and the polymer, facilitating easy recovery of the imprint molecule through mild extraction. For instance, Bahrami reported the first synthesis of IIP NPs using a non-polymerizable ligand "dithizone" (Dz) and applied them for the quantitative and selective separation and enrichment of imprinted Hg^{2+} ions in aqueous solutions.[134] They found that the main binding force between Dz and the polymer network (poly(EGDMA-Dz/Hg(II)) colloidal NPs) is hydrogen bonding.

However, due to the inherent weakness of non-covalent bonds, an excess of functional monomers are often required during polymerization to promote the formation of template-monomer assemblies. The optimal approach to achieve better selectivity, recognition, and binding efficiency involves the use of multiple polymerizable monomers that can simultaneously interact with the imprint molecule.[135–138]

Metal coordination is the most favorable method for ion imprinting due to the robustness and directionality of metal bonds compared to hydrogen bonds.[139] Unlike MIPs, this technique overcomes the limitations associated with nonpolar and aprotic solvents, thereby enabling the use of polar solvents and even aqueous solutions as imprinting media.[140] This capability opens new avenues for the imprinting of biomacromolecules such as proteins, DNA, RNA, antibodies, and biological receptors that typically have low solubility and tendency towards denaturation in organic media.[124]

Careful consideration of the metal ion's characteristics such as its compatibility with the polymerization process, well-defined coordination sphere, and optimal affinity for the template and monomer is essential.[140] A selective and stable interaction between mercury ions and various functional monomers such as 4-vinylpyridine (4-VP) and acrylamide has been recently reported.[141,142] Table 4 summarizes the list of monomers used for the synthesis of Hg-based IIPs. Vinyl group-containing molecules are commonly employed as monomers, as they can easily undergo free radical polymerization. Having one, two or many additional functional groups in molecules such as acrylic acid, pyrrole and thiourea gives them the ability to serve as both functional monomers and complexing agents.[143] They have the ability to form a hydrogen bond and serve as a proton donor and a hydrogen bond acceptor.[144] These multifunctional monomers are generally preferred in IIPs because the presence of functional moieties such as –C=O, –OH and –NH confers excellent coordination capabilities on the monomers.[145]

While numerous monomers hold promising potential for creating IIPs, those with strong and selective binding affinity to Hg species are relatively rare. Although widely used single monomers with multiple functional groups such as MAA and 4-VP exhibit affinity towards mercury and can produce IIPs at a reduced cost,[119] the simultaneous use of multiple monomers (co-monomers) has proven more effective in the imprinting and detection of Hg^{2+}.[147–149] Another common strategy employed to enhance the recognition properties of IIPs is by trapping mercury-selective ligands within the polymer matrix.

Mesa *et al.* employed this approach to evaluate the effectiveness of 2-mercaptobenzimidazole (MBI) and 2-mercaptobenzothiazole (MBT) ligands immobilized in an IIP matrix for the extraction of methyl mercury from water samples.[150] The ligand-based IIPs were synthesized *via* bulk polymerization, involving the initial formation of a pre-polymerization complex by incubating the template (methylmercury), functional monomer (acrylic acid, AA), and the ligand (MBI or MBT) (Fig. 9). Subsequent polymerization produced IIP-MBI-AA and IIP-MBT-AA, exhibiting 53% and 62% methyl mercury sorption respectively. Table 5 gives the schematic illustration of the IIP preparation processes and the Hg^{2+} recognition mechanisms.

Table 4 Polymerizable functional monomers for Hg^{2+}-based IIPs

Uni-functional	Multi-functional			Co-monomers
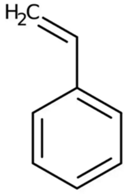 **Styrene (Sty)**	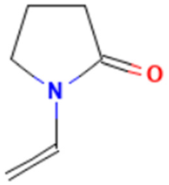 N-vinylpyrrolidine (N-VP)	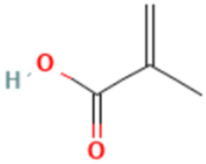 Methacrylic acid (MAA)	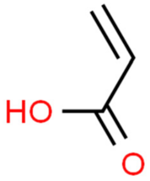 Acrylic acid (AA)	MAA-co-4-VP
	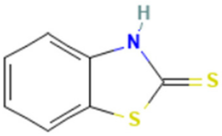 2-mercaptobenzothiazole	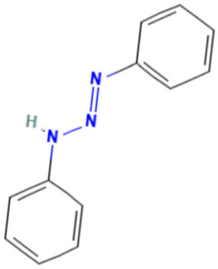 Diazoaminobenzene (DAAB)	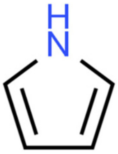 Pyrrole	Sty-co-N-VP
	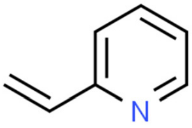 2- or-4-vinylpyridine (VP)	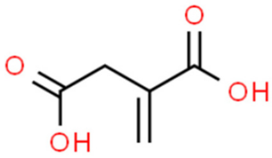 Itaconic acid	1-Amino-8-naphtol-3,6-disodium sulfonate[146]	DAAB-co-4VP

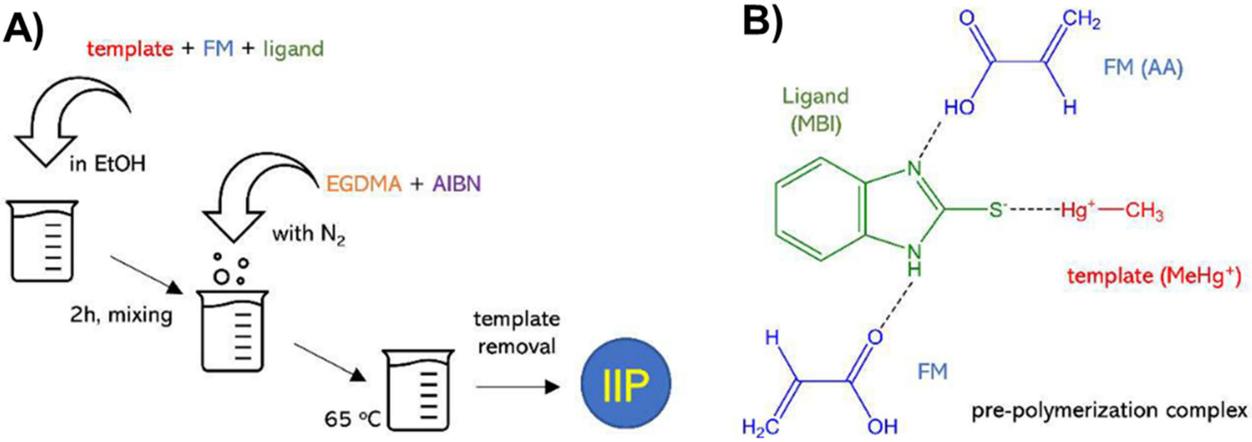

Fig. 9 (A) Schematic illustration of the synthesis of ligand-embedded IIPs. (B) Pre-polymerization complex with the 2-mercaptobenzimidazole (MBI) ligand. Reproduced with permission.[150] Copyright 2020, Multidisciplinary Digital Publishing Institute.

4.2.2. Choice of crosslinkers. The binding capacity and stability of IIPs exhibit a direct correlation with the degree of crosslinking. The amount of crosslinkers plays a pivotal role in generating porosity within copolymer networks. The insufficient incorporation of a crosslinking agent may lead to compromised mechanical stability and render the recognition sites vulnerable to damage, consequently impacting the selectivity of the IIPs.[151] On the contrary, an excessive amount of cross-

Table 5 Mercury recognition and adsorption mechanisms

Mercury adsorption mechanism	Description	Selectivity/ recognition
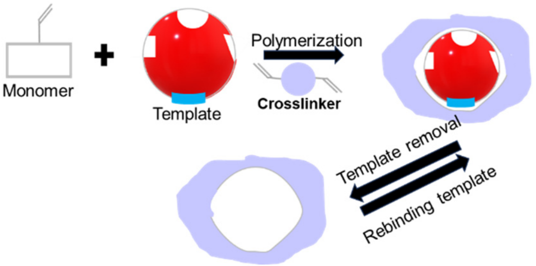	Imprinted polymer made from vinyl monomer only: mercury recognition and adsorption are by shape/size of the imprinted cavity (physisorption)	Low
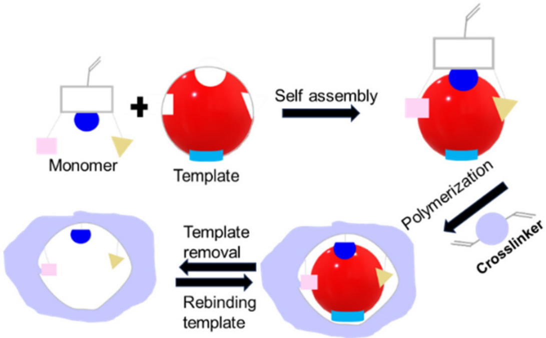	Imprinted polymer made from polymerizable multifunctional monomer: mercury recognition and adsorption are by shape/size of the imprinted cavity and electron donor atoms-to-target interactions (chemisorption and physisorption)	Good
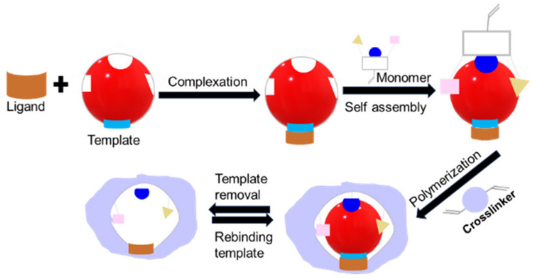	Imprinted polymer made from polymerizable multifunctional monomer with mercury specific ligand entrapped within the IIP/MIP matrix: mercury recognition and adsorption are by imprinted cavity, monomer electron donor atoms, & ligand-to-target complex formation (chemisorption and physisorption)	High

linking agents may result in an IIP characterized by an unusually dense network structure. This, in turn, diminishes its flexibility, mass transfer performance, and the number of recognized adsorption sites per unit mass. Consequently, such conditions can lead to an unsatisfactory adsorption rate and diminished adsorption effectiveness. A comprehensive list of commonly used crosslinking agents is provided in Table 6. These crosslinking agents can be categorized into two groups. The first group comprises agents containing polymeric groups that can undergo copolymerization with monomers. The examples include ethylene glycol dimethacrylate (EGDMA), *N*,*N*′-methylene diacrylamide (MBAA), and divinylbenzene. The second group consists of agents that do not react with themselves but are employed solely to crosslink linear or hyperbranched polymers, such as glutaric dialdehyde and epichlorohydrin (ECH).[130]

4.2.3. Choice of initiators. Most imprinted polymers undergo polymerization through free radicals, photoinitiated polymerization, or electrically initiated polymerization. Among these, free radical polymerization, commonly initiated by heat or light, is the most prevalent method. Initiators such as peroxides and azo compounds, captured in Table 6, are frequently employed. Notably, the compound 2,2′-azobis(2-methyl-propionitrile) (AIBN) is widely used due to its mild reaction conditions with a thermal initiation temperature of 50–70 °C. Critical to this process is the removal of dissolved oxygen from the polymerization system, which inhibits free radical polymerization. Techniques such as ultrasound, vacuum extraction, nitrogen purging, or argon purging are typically employed to eliminate dissolved oxygen.

4.2.4. Choice of solvent (porogenic agent). Solvents, referred to as porogenic agents in IIP synthesis, dissolve reactant species such as template ions, functional monomers, crosslinkers, and initiators. They also control the morphology and porosity of IIPs.[152] During polymerization, solvents evaporate, creating pores. The initial solvent quantity does not affect the polymer mass but significantly influences porosity and hardness. More solvent increases porosity and reduces hardness. Low solvent volume means fewer pores, limiting Hg^{2+} ion access and lowering Hg-IIP adsorption capacity.[152]

Table 6 Summary of MIP methods, components, and performance toward mercury detection

Polymerization method	Ligand	Monomer	Crosslinker	Initiator	Target	Sensor	Detection range	LOD	Sample	Ref.
Bulk	2-MBT	AA	EGDMA	—	$MeHg^+$	IIP-elec.	560–610 μg L^{-1}	538 μg L^{-1}	Water	154
Precipitation	Dithizone	—	EGDMA	AIBN	Hg^{2+}	IIP-elec.	0.5–10 nM 0.08–2 μM	0.1 nM	Water	134
Bulk	4-(2-Thiazolylazo) resorcinol	MAA	EGDMA	AIBN	Hg^{2+}	IIP-elec	4.0×10^{-9}–1.3×10^{-3} mol L^{-1}	1.95×10^{-9} mol L^{-1}	Tuna fish, shrimp, human hair	155
Bulk	Diphenyl thiocarbazone	MAA	EGDMA	AIBN	Hg^{2+}	IIP-spec.	0.2–28 μg L^{-1}	0.05 μg L^{-1}	Serum	156
Bulk	—	DAAB and VP	EGDMA	AIBN	Hg^{2+}	IIP-(CVAAS)	0.13 to 25 μg L^{-1}	0.05 μg L^{-1}	Tap, river, and sea water	157
Bulk	MBI, MBT	AA	EGDMA	AIBN	$MeHg^+$	IIP-AA	—	159 μg g^{-1}, 457 μg g^{-1}	Water	150
Surface imprinting	—	2-MBT	—	—	Hg^{2+}	IIP-elec.	1–160 nM	0.1 nM	Water	158
Solid phase extraction	—	2-VP	EGDMA	AIBN	Hg^{2+}	IIP-AAS	—	0.5 pg mL^{-1}	Water, fish	15
Bulk poly	—	Styrene (Sty), NVP, Sty-co-NVP	EGDMA	AIBN	Hg^{2+}	IIP-elec.	90–10 ppm	2 ppm (Sty), 1 ppm (Sty-co-NVP)	Water	136
Surface imprinting	2,2′-((9*E*,10*E*)-1,4-Dihydroxyanthracene-9,10-diylidene) bis(hydrazine-1-carbothioamide)	MAA	EGDMA	AIBN	Hg^{2+}	IIP-elect.	0.07 to 80 μg L^{-1}	0.02 μg L^{-1}	Water	159
Bulk	—	(4-Ethenylphenyl)-4-formate-6-phenyl-2,2′-bipyridine	Divinylbenzene	AIBN	$MeHg^+$	MIP-(CVAAS)	0.093–22 μg L^{-1}	0.041 μg L^{-1}	Human hair and soil	141
Bulk	—	HEMA & MAC co monomers	EGDMA	Benzoyl peroxide	Hg^{2+}	IIP-(CVAAS)	—	0.45 mg Hg^{2+} per g	Human serum	160
Bulk	Dithizone	MAA	EGDMA	AIBN	Hg^{2+}	IIP-(CV AFS)		0.02 μg L^{-1}	Water	161
Bulk	—	VP	EDMA	AIBN	Hg^+	IIP-elec.	$2.5 \times {}^{-9}$ to $5.0 \times {}^{-7}$	$5.2 \times {}^{-10}$ M	Water	143
Bulk	—	MAA	TMPTMA	AIBN	Hg^{2+}	IIP-CVAAS	—	0.006 μg L^{-1}	Water	162
Bulk	—	Pyrrole	EGDMA	Sodium persulfate	Hg^{2+}	IIP-elect.	0.09–20.05 mg L^{-1}	0.02 mg L^{-1}	Water	13
Bulk	—	Sodium carboxymethyl cellulose	Epichlorohydrin	—	Hg^{2+}	IIP-elec.	20–800 μg L^{-1}	0.1 μg L^{-1}	Water	163
Precipitation	—	Itaconic acid	EGDMA	AIBN	Hg^{2+}	IIP-elec.	0.1–20 nM	29 pM	Water	164

Abbreviations: acrylic acid (AA), methacrylic acid (MAA), diazoaminobenzene (DAAB), vinylpyridine (VP), *N*-vinylpyrrolidone (NVP), hydroxyethyl methacrylate (HEMA), *N*-methacryloyl-(L)-cysteine (MAC), trimethylolpropane trimethacrylate (TMPTMA), 2,2′-azobisisobutyronitrile (AIBN), ethylene glycol dimethacrylate (EGDMA), 2-mercaptobenzimidazolate (MBI), 2-mercaptobenzothiazole (MBT), cold vapor atomic fluorescence spectrometry (CV AFS), cold vapor atomic absorption spectrometry (CVAAS).

Solvents fall into two categories: non-polar, aprotic (*e.g.*, chloroform and acetonitrile) and polar, protic (*e.g.*, methanol and water). Despite toxicity and storage challenges, non-polar solvents are preferred for effective template-functional monomer association.[153] Non-polar solvents such as toluene or hexane excel in pre-polymerization reactions, yielding IIPs with a non-polar surface chemistry, promoting Hg^{2+} ion physisorption.[153] Polar solvents, while mild and non-toxic, disrupt noncovalent interactions, which inform their less use in IIP synthesis.

4.3. Applications of IIPs

The IIPs have been used in various formats such as bulk materials, thin films, NPs, and sensors. IIPs play a dual role in detecting and removing heavy metals, such as mercury species. Bulk IIPs have been used for solid-phase extraction to remove mercury from numerous environmental samples. Furthermore, thin-film IIPs have been used for surface imprinting and sensing applications.[146] For mercury removal or sorption, first, the presence of mercury in the sample has to be confirmed by some other means such as AAS equipment. The time consumption and complexity of this process have led to a more elegant approach, where the selective adsorption of IIPs for mercury has been harnessed to develop a platform with capability to recognize, adsorb and simultaneously provide detection signals corresponding to the amount of Hg compounds in an environmental sample without the use of any complex external equipment. This multifunctional mercury detection and removal capability make IIP technique stand out from other mercury detection sensors such as SERS, electrochemical and colorimetric sensors.

This section will focus on the construction IIP sensors and the application of IIPs for mercury detection and mercury removal *via* sorption, highlighting the performances of recent approaches, and the materials and methods used.

4.3.1. IIPs for Hg^{2+} detection. The construction of an IIP chemical sensor for mercury detection is a multi-step process that involves the integration of various components to create a functional sensing device. The development of such sensors is crucial for applications in environmental monitoring, medical diagnostics, industrial process control, and food safety.

Chemical sensors, as devices designed to identify and quantify specific chemical substances or changes in chemical concentrations, require the integration of key components. These include recognition elements, which can be biological (enzymes, aptamers, and antibodies), or chemical receptors like IIPs with specific binding sites for target analytes. Another fundamental component is the transducer, responsible for converting the recognition event into a measurable signal. Transduction methods vary and can include electrochemical, optical, piezoelectric, or resistive approaches. For example, electrochemical transducers measure changes in electrical properties, while optical transducers utilize alterations in light absorption, fluorescence, or refractive index. Following transduction, a signal processing unit comes into play. This unit amplifies, filters, and processes the raw signal to enhance sensitivity and selectivity. The processed signal is then presented through an output display or interface, offering quantitative information about the detected analyte in a user-friendly manner. These components work together synergistically to create effective chemical sensors capable of accurate and reliable detection and quantification of target substances in various applications.

In the context of IIP-based sensors for mercury detection, the immobilization of IIPs on transducers such as quartz crystal microbalance, electrodes, or SPR platforms is a common practice. The binding of the target molecule to IIPs induces changes in the physical or chemical properties of the transducer, which are then detected by the sensor and displayed through the output display or interface. This integrated approach allows for the fabrication of a cohesive and effective chemical sensor for mercury detection. For example, Hande *et al.* prepared IIPs using a monomer with fluorescence property that is quenched in the presence of a Hg^{2+} ion due to intermolecular charge transfer from oxygen and nitrogen atoms of the monomer to the Hg^{2+} ion.[165] By polymerizing their pioneered fluorescence monomer (*N*-[4-(2-oxo-2*H*-chromen-3-yl)-thiazol-2-yl]-acrylamide) in the presence of EGDMA (crosslinker), AIBN (initiator), and a Hg^{2+} template, an IIP was achieved with high affinity to Hg^{2+} ions. The fluorescence responded in the linear range of 0.05–1.2 μmol L^{-1} with a detection limit of 0.020 μmol L^{-1}.

In another pioneering work using pyrrole for the first time as a functional monomer, the electrochemical analysis of Hg^{2+} in real water sample was achieved using differential pulse anodic stripping voltammetry (DPASV).[13] The Hg-IIP was synthesized using EGDMA as a crosslinker agent and sodium persulfate as an initiator. The proposed methodology presents a limit of detection (LOD) of 0.02 mg L^{-1} within a linear range of 0.09 mg L^{-1} to 20.05 mg L^{-1}.

More recent methods combine ion imprinting with nanomaterials to develop a sensor with high efficiency and sensitivity for ion or molecular detection and removal by leveraging the high surface area and good electrical properties of nanomaterials.[166] Nanomaterial supports such as those of Fe_3O_4,[167] reduced graphene oxide,[159] $Fe_3O_4@SiO_2$,[133] and core–shell $Fe_3O_4@SiO_2@TiO_2$ [156] have been used in IIPs. For example, Soman *et al.*, reported the development of an electrochemical-IIP sensor based on graphene quantum dots covalently linked to thiourea functional monomers (Fig. 10A and B).[168] The sensor showed high selectivity for Hg^{2+} ions in the linear range of 5×10^{-8} M to 2.3×10^{-5} M, and an LOD of 23.5 nM in differential pulse voltammetry. Cyclic voltammetry showed linear response ranges of 6×10^{-8} to 8.5×10^{-7} and 1.4×10^{-6} to 7×10^{-6} M with an LOD of 30.2 nM in real water samples. Jiang *et al.* synthesized MeHg ion-imprinted magnetic NPs to specifically detect and extract ultra-trace MeHg from water samples (Fig. 10C).[133] The MeHg IIP employed magnetic core–shell $Fe_3O_4@SiO_2$ NPs as supporting structures, the complex ion of 1-pyrrolidinecarbodithioic acid and MeHg as a template, MAA as a functional monomer and trimethylolpropane trimethacrylate as a crosslinker. The IIP achieved an LOD of

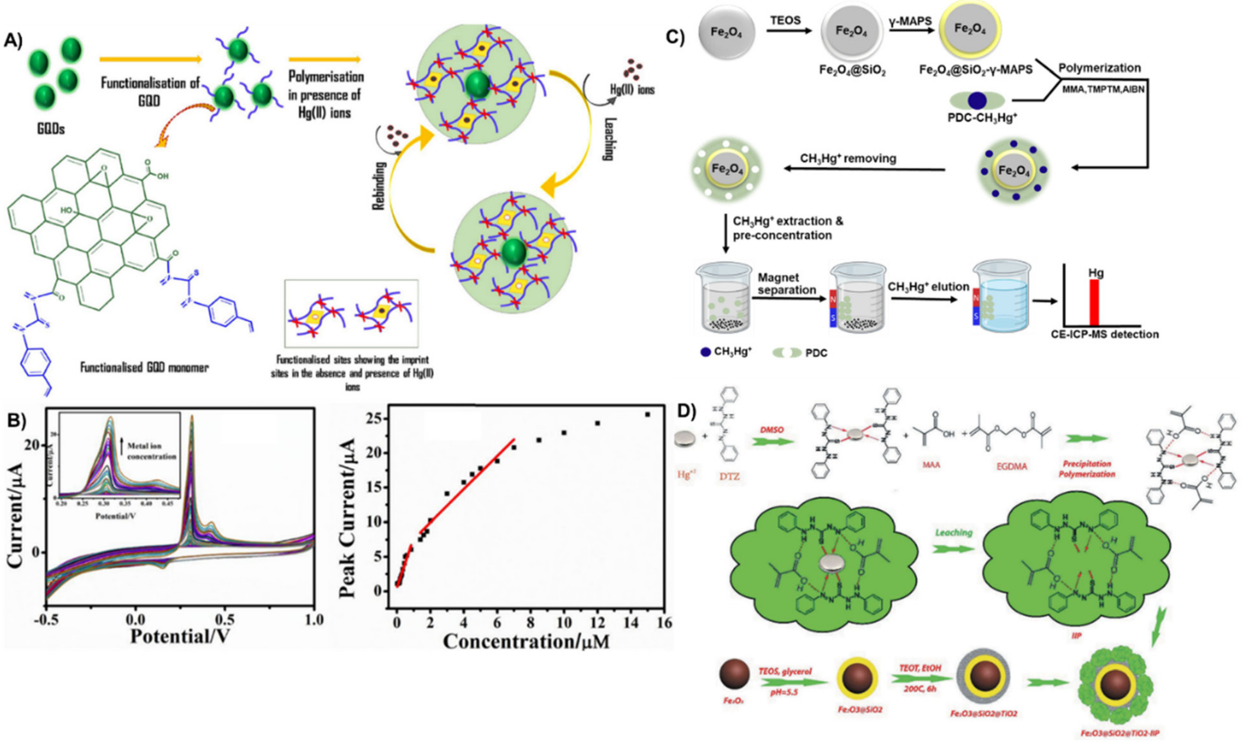

Fig. 10 (A and B) Synthesis of the imprinted polymer material graphene quantum dot thiourea-IIP with the cyclic voltammograms of the sensor (B left) in response to 60 × 10^{-9} M to 15 × 10^{-6} M Hg^{2+} (100 mV s^{-1} scan rate) and calibration graph (B right). Reproduced with permission.[168] Copyright 2021, Journal of Polymer Research. (C) Experimental principle of preparing MeHg-ion imprinted magnetic NPs (MeHg IIMN) and detecting MeHg in water samples using CE-ICP-MS together with MeHg IIMN. Reproduced with permission.[133] Copyright 2017, Elsevier. (D) Schematic representation of the synthesis of Fe_3O_4@SiO_2@TiO_2-IIP for mercury ion separation. Reproduced with permission.[156] Copyright 2019, Separation Science and Technology.

0.084 pg mL^{-1}, a maximum adsorption of 25 mg MeHg per g within 30 min and 50 times recyclability without any loss of performance.

In a novel ultrasonically assisted spectrophotometric method, an IIP immobilized on magnetic NPs was used to achieve selective detection, separation, and pre-concentration of Hg^{2+} ion targets in a matrix of samples containing interferents (Fig. 10D).[156] The core–shell adsorbent (Fe_3O_4@SiO_2@TiO_2) acts as a stabilizer to the polymer and enhances the sensitivity efficiency, allowing for the easy separation of Hg^{2+} using an external magnetic field. The detection and adsorbent system showed a linear dynamic range and a limit of detection of 0.20–28.00 μg L^{-1} and 0.05 μg L^{-1} respectively.

Alizadeh *et al.* utilized IIPs immobilized on a graphite paste electrode that was modified with multi-walled carbon nanotubes (MWCNTs) for the detection of mercury in environmental water.[164] The IIP-Hg-NPs were synthesized *via* precipitation polymerization using itaconic acid as a functional monomer. First, a carbon paste electrode was impregnated with the synthesized Hg-IP-NPs and MWCNTs. Mercury ions were then accumulated on the electrode surface *via* an open circuit procedure where Hg^{2+} ions were reduced to their metallic form at a negative pre-potential using square-wave anodic stripping voltammetry to generate the electrochemical signal. The high affinity of the Hg-IP-NPs for Hg^{2+} was substantiated by comparing the signals of electrodes with imprinted and non-imprinted polymers. The electrode's sensitivity to Hg^{2+} (enhanced by the MWCNTs) showed a linear response in the range of 0.1–20 nM and an LOD of 29 pM.

Among the limited reports available for mercury detection using IIPs, IIP-electrochemical sensors emerge as the most common type, and are increasingly recognized as alternatives to spectroscopic techniques for detecting Hg^{2+}. This popularity stems from their high sensitivity, portability, low cost, simple instrumentation, and ability to provide real-time analysis. However, the electrochemical method encounters challenges related to polymer matrix interferences. Consequently, separation and preconcentration procedures are often necessary before the determination step. While the high adsorption capacities of IIPs contribute to improved sensitivity and lower detection limits, enhancing the selectivity for a specific element remains an area for improvement. Efforts directed towards enhancing the selectivity of IIP-based electrochemical sensors can lead to more reliable and accurate detection of mercury ions, further advancing their applicability in environmental monitoring and analytical chemistry.

4.3.2. IIPs for mercury capture and removal. While various methods exist for mercury capture and removal, solid-phase extraction (SPE), particularly using IIPs, stands out for its flexibility, cost-effectiveness, environmental friendliness, speed, simplicity, and versatility in adsorption, separation, and preconcentration processes. Despite the widespread adoption of SPE, the selectivity of solid support materials such as active carbon, ion-exchange resins, chelating fibers, and chelating resins can still be improved for certain elements. Consequently, IIPs have emerged as a novel SPE approach for the direct and selective removal of metal ions including Hg^{2+}. Their advantages include the need for a small quantity of polymers, reusability, and easy preparation, making them compatible with traditional analytical instruments such as AAS, CVAAS, HPLC, ICP-OES and modern electrochemical, SPR and SERS platforms.

For example, Liu *et al.* reported the development of an MIP tailored for methylmercury determination and analysis using CVAAS.[141] Initially, the MIP was crafted through the formation of a monomer complex involving methylmercury and (4-ethenylphenyl)-4-formate-6-phenyl-2,2′-bipyridine. Subsequently, thermal polymerization with divinylbenzene (as the crosslinker) occurred in the presence of 2,2′-azobisisobutyronitrile as the initiator. The template was then removed using an acidic thiourea solution. This MIP exhibited notable attributes, featuring a higher adsorption capacity of 170 μmol g^{-1} and an LOD of 0.041 μg L^{-1}, while showcasing superior selectivity for methylmercury in comparison to non-imprinted polymers. The selective factor (α_r) values for CH_3Hg^+/Hg^{2+}, CH_3Hg^+/Cu^{2+}, CH_3Hg^+/Zn^{2+}, and CH_3Hg^+/Cd^{2+} were 24.0, 46.7, 50.7, and 40.2, respectively, all surpassing 1 which indicates that the selective removal of methylmercury can be done even when the coexisting metal ions are present. Moreover, the methylmercury-imprinted polymers demonstrated reusability over at least twenty cycles, consistently achieving recoveries of no less than 95%. Table 7 showcases the efficacy of IIPs in mercury adsorption across different monomers and mercury-selective ligands.

Basir and colleagues successfully removed mercury ions from water by synthesizing Hg^{2+}-imprinted polymers (Hg-IIPs) with a silica core *via* radical polymerization.[169] They used complexes of Hg^{2+} ions with 3-mercaptopropyltrimethoxysilane ligands as templates, with vinyl-trimethoxysilane as a monomer and ethylene glycol dimethacrylate as a crosslinker in a molar ratio of 1/6/6. The approach involved trapping Hg^{2+} ions in a polymer matrix using 3-mercaptopropyltrimethoxysilane (MPTS) ligands. The SH groups in the ligand formed covalent bonds with Hg^{2+} ions, while the other side of the ligand bound to the silica core through hydrolysis. When Hg-IIPs were used as the sorbent, optimal removal of mercury ions was achieved in a batch at pH 4, with an interaction time of 90 minutes, resulting in a notable adsorption capacity of 62.27 mg g^{-1}. In the presence of Pb(II), Cd(II), and Cu(II) ions in quaternary solutions, Hg-IIPs exhibited remarkable selectivity, with selectivity coefficients of 46.92 for Hg/Cu, 16.82 for Hg/Cd, and 2.07 for Hg/Pb. The analysis was done using CVAAS.

Mergola *et al.* detailed the preparation of IIPs designed for the selective removal of Hg^{2+} ions from aqueous media using 4-VP (monomer), EGDMA (crosslinker), AIBN (initiator), and 4/1, v/v acetonitrile/water as porogens.[170] Two synthesis approaches were employed to investigate the impact of diphenylcarbazone (DPC), a non-polymerizable ligand, on the absorption performance. Initially, bulk polymerization was utilized to create two polymers, namely, IIP1 and IIP2, in the absence and presence of DPC. The incorporation of DPC in IIP2 facilitated the formation of ternary complexes with mercury ions. Additionally, 4-vinylpyridine monomer induced an enhancement in binding performance, evident in the high-affinity binding sites of IIP1 and IIP2, as reflected by their K_a values ($1.7 \times 10^3 \pm 0.4$ M^{-1} and $12.1 \times 10^3 \pm 0.5$ M^{-1}, respectively). A third polymer, IIP3, was synthesized using precipitation polymerization to assess the influence of morphological characteristics on the absorption performance in comparison to the addition of DPC. Competitive studies underscored a more pronounced impact of IIP3 morphology on selectivity performance, with the formation of monodisperse microbeads observed exclusively in this case. Finally, the practical application of the polymers was demonstrated through batch experiments involving drinking water spiked with 1 μg mL^{-1} of Hg^{2+} ions. Among the tested polymers, IIP2 exhibited the highest removal efficiency, nearing 80%.

Esmali *et al.* have recently developed a highly selective approach for Hg^{2+} adsorption by combining ionic imprinted

Table 7 Overview of the adsorption efficiency of IIPs for mercury, considering different monomers and ligands

Monomer	Ligand	Analyte	Adsorption capacity (mg g^{-1})	Analyte recovery (%)	Time	Reusability	Ref.
DVB	(4-Ethenylphenyl)-4-formate-6-phenyl-2,2′-bipyridine	$MeHg^+$	42.68	95.0	24 h	20 times	141
VTMS	MPTS	Hg^{2+}	62.27	—	90 min	—	169
4-VP	DPC	Hg^{2+}	70.00	80.0	60 min	—	170
Ether sulfone	Bathophenanthroline	Hg^{2+}	21.60	98.1	12 h	6 times	171
3-Vinyletriethoxy silane	*N*-(Pyridin-2-ylmethyl) ethenamine	Hg^{2+}	147.00	98.3	2 min	—	167
Methacrylic acid	PDC	$MeHg^+$	25.00	95.0	30 min	50 times	133

Abbreviations: divinylbenzene (DVB), 3-mercaptopropyltrimethoxysilane (MPTS), diphenylcarbazone (DPC), 1-pyrrolidinecarbodithioic acid (PDC), vinyl-trimethoxysilane (VTMS).

polymers with membranes.[171] They obtained poly(ether sulfone)-based ion-imprinted membranes (IIMs) *via* phase inversion, using IIP particles produced *via* radical copolymerization of acrylamide, acrylonitrile, and EGDMA, along with a Hg^{2+} template complexed with bathophenanthroline. The study, which employed central composite design (CCD) in conjunction with response surface methodology (RSM), investigated the removal of Hg^{2+} from water and the pure water flux of the IIM. The results demonstrated an impressive removal efficiency of 98.1% and a flux of 37.5 kg m^{-2} h^{-1}. Notably, the IIM exhibited a maximum adsorption capacity of 432 mg m^{-2} (or 21.6 mg g^{-1}), nearly four times higher than that of the non-imprinted membrane (NIM; 105 mg m^{-2} or 5.25 mg g^{-1}), prepared without the Hg^{2+} template. Furthermore, the IIM displayed remarkable selectivity for Hg^{2+} ions over other metal ions and proved to be recyclable for at least 6 cycles without any significant loss of adsorption capacity.

The common problems associated with MIP/IIP handling such as the need for filtration and centrifugation to separate the polymer from the solution, which often led to significant loss of polymer during filtration, are generally overcome by using magnetically active particles for easy separation using a magnet. For example, a magnetic sorbent IIP based on *N*-(pyridin-2-ylmethyl)ethenamine coated on Fe_3O_4 NPs was investigated for the rapid extraction, preconcentration and also determination of trace amounts of Hg^{2+} ions in fish samples by inductively coupled plasma-optical emission spectrometry (ICP-OES). The maximum adsorption capacity of this sorbent was 147 ± 2 mg g^{-1} with an LOD found to be 0.03 ng mL^{-1}.[167]

Jiang *et al.* successfully developed MeHg ion-imprinted magnetic NPs (MeHg-IIMNs) for the rapid and specific extraction/concentration of ultra-trace MeHg from natural water samples, achieving results within just 30 minutes.[133] The MeHg IIMN used core–shell $Fe_3O_4@SiO_2$ NPs ($Fe_3O_4@SiO_2$ NPs) as robust supporting structures. The complex ion of 1-pyrrolidinecarbodithioic acid and MeHg ($PDC\text{-}CH_3Hg^+$) served as the template, with methacrylic acid acting as the functional monomer and trimethylolpropane trimethacrylate as the cross-linker. Impressively, the adsorbent demonstrated a maximum adsorption capacity of 25 mg MeHg per g, with the ability to recycle up to 50 times while maintaining a recovery rate greater than 95%. Notably, the adsorbent exhibited minimal interference from other ions. Using electrophoresis-inductively coupled plasma mass spectrometry (CE-ICP-MS), the adsorbent achieved a low detection limit (LOD) of 0.084 pg mL^{-1} for MeHg.

The sorption efficiency of IIPs can greatly be improved by optimizing IIP synthesis conditions such as pH, analyte-IIP incubation time, and temperature. For example, pH values ranging between 4 and 8 are reported to be suitable for enhanced mercury adsorption. At pH < 4, the ability of IIPs to detect or remove Hg is diminished, because active groups such as SH, C=O, and –NH in sorbents/ligands undergo protonation due to the high concentration of H^+ ions in the solution. This makes the sorbent surfaces positively charged, causing electrostatic repulsion of the positively charged mercury ions.[169] At a pH value >8, the mercury ions begin to form hydroxylated complexes, and the number of OH^- and $Hg(OH)_2$ in the solution increases, which make it difficult for the major Hg^{2+} species to bind to the IIP sites, hence reducing the detection and removal of the mercury ions.[116,141]

The effect of time could also manifest in the adsorption rate of Hg(II) ions at the available binding sites of the IIP, which generally occur in 3 phases: the rapid phase that occurs within the first 15 minutes is characterized by a high affinity of active groups of the sorbent to Hg(II) ions, due to sufficient capacity. At the slow phase, the sorption rate slows down leading to the third phase where equilibrium is reached. At this stage, the adsorption of mercury ions to the surface ceases due to the saturation of the sorbent surface by mercury ions.[169]

Ion imprinting indeed presents a promising technique for developing materials geared towards the detection and removal of mercury from environmental samples. The use of IIPs can offer high selectivity and sensitivity for mercury ions, rendering them valuable for environmental monitoring and remediation. However, further research is warranted to optimize the synthesis conditions and validate the performance of IIPs in real-world applications. Through continued development and optimization, ion imprinting holds the potential to evolve into a valuable tool for onsite detection and removal of heavy metals from the environment, thus contributing significantly to environmental protection and human health preservation efforts.

5. Conclusion and future directions

In conclusion, SERS and MIPs/IIPs demonstrate significant potential and practical applications in the detection and removal of mercury from various environmental and human samples, including spanning water, soil, food, and blood. The exceptional sensitivity of SERS and the specific recognition and affinity of IIPs for Hg^{2+} render them promising candidates as efficient methods to determine and identify mercury species in real samples. However, a critical analysis of the existing literature reveals several gaps and areas for future exploration:

- *Limited synthesis and use of new mercury-specific ligands in SERS*: the synthesis, study, and use of new mercury-specific ligands in SERS are underreported, despite traditional ligands lacking exclusive selectivity for mercury and struggling to discriminate between different mercury species.
- *Focus on Hg^{2+} species in sensors*: most sensors reported in the literature primarily target Hg^{2+} species, neglecting MeHg, which is considered the most hazardous form of mercury.
- *Underexplored validation of IIPs in real-world applications*: the validation of IIPs for real-world applications including the detection and removal of mercury species from complex environmental samples such as seawater and industrial wastewater has received limited attention. Further studies are required to assess IIPs' performance under diverse environ-

mental conditions and optimize them for specific applications.

- *Imbalance in electrochemical-IIP vs. IIP-SERS sensor development*: there are a significant number of reports on the development of electrochemical-IIP sensors for mercury detection, while information on IIP-SERS sensors is comparatively scarce.

Addressing these gaps through focused research efforts can enhance the efficacy and applicability of both SERS and IIPs in mercury detection and removal, thereby contributing to improved environmental monitoring and human health protection strategies. Considering these observations, future research efforts are suggested to direct towards:

- *Exploration of mercury-specific ligands*: more attention should be paid to exploring and synthesizing new mercury-specific ligands that can be incorporated into SERS or IIP detection platforms. These ligands should exhibit high selectivity and sensitivity towards different mercury species including Hg^{2+} and MeHg.
- *Development of SERS-IIP hybrid sensors*: efforts should be made to develop SERS-IIP hybrid sensors to address the limitations of each technique individually. This strategic combination could leverage the high sensitivity of SERS and the selective adsorption capabilities of IIPs. Achieving synergy between these two techniques could represent a groundbreaking advancement, providing a sensitive and selective tool for on-site mercury detection.
- *Advanced computation-assisted development*: machine learning (ML) technique has been increasingly used for bio/sensor development including SERS[172] and MIP/IIP.[121,173] Hence, the integration of ML offers promising opportunities for advancing and facilitating the design, optimization, and applications of SERS and MIP/IIP platforms, particularly for mercury detection in complex samples.

Despite the current gaps, the practical application of IIPs and SERS in detecting and removing mercury species from the environment remains promising and holds good prospects for future advancements. Collaborative research efforts across multidisciplinary fields can accelerate progress in this direction, ultimately contributing to improved environmental monitoring and remediation, and human health protection.

Author contributions

Conceptualization, Jianjun Wei; funding acquisition, Simona Murph and Jianjun Wei; investigation, Frank Tukur, Panesun Tukur and Jianjun Wei; project administration, Jianjun Wei; resources, Simona Murph and Jianjun Wei; supervision, Simona Murph and Jianjun Wei; writing – original draft, Frank Tukur and Panesun Tukur; writing – review & editing, Simona Murph and Jianjun Wei.

Conflicts of interest

There are no conflicts to declare.

Acknowledgements

This work was supported by the Department of Energy Minority Serving Institution Partnership Program (MSIPP) managed by the Savannah River National Laboratory under BSRA contract SOW # G-SOW-A-02425 (TOA number: 0000602834).

References

1 J. Briffa, E. Sinagra and R. Blundell, *Heliyon*, 2020, **6**, e04691.
2 D. D. Gummin, J. B. Mowry, M. C. Beuhler, D. A. Spyker, L. J. Rivers, R. Feldman, K. Brown, P. T. P. Nathaniel, C. Alvin, J. A. Weber, D. D. Gummin, J. B. Mowry, M. C. Beuhler, D. A. Spyker, L. J. Rivers, R. Feldman, K. Brown, P. T. P. Nathaniel, A. C. Bronstein, D. D. Gummin, J. B. Mowry, M. C. Beuhler, D. A. Spyker, L. J. Rivers and R. Feldman, *Clin. Toxicol.*, 2022, **60**, 1381–1643.
3 H. Wu, G. Lin, C. Liu, S. Chu, C. Mo and X. Liu, *Trends Environ. Anal. Chem.*, 2022, **36**, e00178.
4 P. Grandjean, H. Satoh, K. Murata and K. Eto, *Environ. Health Perspect.*, 2010, **118**, 1137–1145.
5 P. Li, X. Feng and G. Qiu, *Int. J. Environ. Res. Public Health*, 2010, **7**, 2666–2691.
6 UN Environment, *Global Mercury Assessment 2018: Key Findings*, 2019.
7 A. Philibert, M. Fillion, J. Da Silva, T. S. Lena and D. Mergler, *Environ. Health*, 2022, **21**, 34.
8 Y. Zhang, Z. Song, S. Huang, P. Zhang, Y. Peng, P. Wu, J. Gu, S. Dutkiewicz, H. Zhang, S. Wu, F. Wang, L. Chen, S. Wang and P. Li, *Nat. Commun.*, 2021, **12**, 3035.
9 Y. Gao, Z. Shi, Z. Long, P. Wu, C. Zheng and X. Hou, *Microchem. J.*, 2012, **103**, 1–14.
10 S. Botasini, G. Heijo and E. Méndez, *Anal. Chim. Acta*, 2013, **800**, 1–11.
11 WHO, *WHO/SDE/WSH/05.08/10*.
12 D. K. Sarfo, A. Sivanesan, E. L. Izake and G. A. Ayoko, *RSC Adv.*, 2017, **7**, 21567–21575.
13 G. Islas, L. E. Rebolledo-perales, I. Ibarra, M. Franco and A. Alvarez, *Electrochim. Acta*, 2022, **434**, 141258.
14 World Health Organization, *Guidelines for drinking-water quality*, 2022.
15 M. Soleimani and M. G. Afshar, *J. Anal. Chem.*, 2015, **70**, 5–12.
16 Mercury Exposure and Toxicity, Report by the Office of Public Health, Louisiana Department of Health, 2023.
17 J. M. González-Rubio, N. Domínguez-Morueco, S. Pedraza-Díaz, A. C. Portilla, M. Á. Lucena, A. Rodriguez, A. Castaño and M. Esteban-López, *Environ. Int.*, 2023, **177**, 107958.
18 M. Atasoy, D. Yildiz, İ. Kula and A. İ. Vaizoğullar, *Food Chem.*, 2023, **401**, 134152.

19 G. da S. Coelho Junior, D. L. G. Borges, M. Svoboda, J. Dědina and J. Kratzer, *Spectrochim. Acta, Part B*, 2023, **200**, 106596.

20 Y. Vicente-Martínez, M. J. Muñoz-Sandoval, M. Hernandez-Cordoba and I. Lopez-Garcia, *Molecules*, 2023, **28**, 14.

21 F. A. da Silva Cunha, M. J. de Oliveira, P. P. Florez-Rodriguez and J. C. C. Santos, *Spectrochim. Acta, Part B*, 2022, **192**, 106412.

22 R. Li and X. Deng, in *IOP Conference Series: Earth and Environmental Science*, 2020, vol. 440, p. 042047.

23 M. L. Astolfi, C. Protano, E. Marconi, D. Piamonti, L. Massimi, M. Brunori, M. Vitali and S. Canepari, *Microchem. J.*, 2019, **150**, 104186.

24 A. Sabouri and S. Nouroozi, *RSC Adv.*, 2016, **6**, 80354–80360.

25 M. Winter, F. Lessmann and V. Harth, *Anal. Methods*, 2023, **15**, 2030–2038.

26 K. Ilmiah, J. Sumranjit, T. Wutikhun and A. Siripinyanond, *ACS Appl. Nano Mater.*, 2022, **6**, 1250–1260.

27 S. H. Choi, J. Y. Kim, E. Mi Choi, M. Y. Lee, J. Y. Yang, G. Ho Lee, K. Su Kim, J. S. Yang, R. E. Russo, J. H. Yoo, G. J. Kang and K. Su Park, *Anal. Lett.*, 2019, **52**, 496–510.

28 H. Xiao, W. Wang, S. Pi, Y. Cheng and Q. Xie, *Sens. Actuators, B*, 2020, **317**, 128202.

29 T. T. K. Nguyen, H. T. Luu, L. D. Vu, T. T. Ta and G. T. H. Le, *J. Chem.*, 2021, **2021**, 8888879.

30 Q. Li, H. Li, K. Li, Y. Gu, Y. Wang, D. Yang and Y. Yang, *J. Hazard. Mater.*, 2023, **441**, 129919.

31 S. An, F. Zeeshan, B. Norlin and G. Thungstrom, *IOP Conf. Ser. Earth Environ. Sci.*, 2021, 690, 012031.

32 D. J. Butcher, *Appl. Spectrosc. Rev.*, 2016, **51**, 397–416.

33 S. Ali, M. Mansha, N. Baig and S. Akram, *Chem. Rec.*, 2022, **22**, e202100327.

34 Y. Du, R. Liu, B. Liu, S. Wang, M. Han and Z. Zhang, *Anal. Chem.*, 2013, **85**, 3160–3165.

35 Z. Gul, S. Ullah, S. Khan, H. Ullah, M. U. Khan, M. Ullah, S. Ali and A. A. Altaf, *Crit. Rev. Anal. Chem.*, 2024, **54**, 44–60.

36 R. D. Ayivi, B. O. Adesanmi, E. S. McLamore, J. Wei and S. O. Obare, *Chemosensors*, 2023, **11**, 203.

37 R. D. Ayivi, S. O. Obare and J. Wei, *TrAC, Trends Anal. Chem.*, 2023, **167**, 117231.

38 P. D. Selid, H. Xu, E. M. Collins, M. S. Face-collins and J. X. Zhao, *Sensors*, 2009, **9**, 5446–5459.

39 C. T. Driscoll, R. P. Mason, H. M. Chan, D. J. Jacob and N. Pirrone, *Environ. Sci. Technol.*, 2013, **47**, 4967–4983.

40 Y. Liu, H. Chen, N. Zhu, J. Zhang, Y. Li, D. Xu, Y. Gao and J. Zhao, *Environ. Pollut.*, 2022, **293**, 118557.

41 S. C. T. Nicklisch, L. T. Bonito, S. Sandin and A. Hamdoun, *Environ. Pollut.*, 2017, **229**, 87–93.

42 C. J. Murphy, A. M. Gole, S. E. Hunyadi and C. J. Orendorff, *Inorg. Chem.*, 2006, **45**, 7544–7554.

43 C. Song, J. L. Abell, Y. He, S. Hunyadi Murph, Y. Cui and Y. Zhao, *J. Mater. Chem.*, 2012, **22**, 1150–1159.

44 S. E. Hunyadi and C. J. Murphy, *J. Mater. Chem.*, 2006, **16**, 3929–3935.

45 S. E. H. Murph, G. K. Larsen and K. J. Coopersmith, *Anisotropic and shape-selective nanomaterials: structure-property relationships*, Springer, 2017.

46 T. S. Srivatsan, W. C. Harrigan and S. E. Hunyadi Murph, *Metal-Matrix Composites: Advances in Analysis, Measurement, and Observations*, Springer Nature, 2021.

47 S. E. Hunyadi Murph, K. J. Heroux, C. E. Turick, D. Thomas, in *Applications of Nanomaterials*, Studium Press LLC, 2012, pp. 7823–7830.

48 M. S. S. Bharati and V. R. Soma, *Opto-Electron. Adv.*, 2021, **4**, 210048.

49 F. Tukur, B. Bagra, A. Jayapalan, M. Liu, P. Tukur and J. Wei, *ACS Appl. Nano Mater.*, 2023, **6**, 2071–2082.

50 K. Rhee, A. Tukova and Y. Wang, *Nanoscale*, 2023, **15**, 2087–2095.

51 Y. Ying, Z. Tang and Y. Liu, *Nanoscale*, 2023, **15**, 10860–10881.

52 C. Zong, C. Chen, M. Zhang, D. Wu and B. Ren, *J. Am. Chem. Soc.*, 2015, **137**, 11768–11774.

53 S. Schultz, T. D. Payne and S. H. Kim, *Sens. Diagn.*, 2023, **2**, 1483–1491.

54 W. Xiao, M. Xiao, Q. Fu, S. Yu, H. Shen, H. Bian and Y. Tang, *Sensors*, 2016, **16**, 1871.

55 W. Kim, W. Kim, D. Bang, J. Park and W. Lee, *Chemosensors*, 2023, **11**, 340.

56 X. Zheng, L. Zhang, L. Huang, W. Li, R. Song, L. Chen and H. Zeng, *ACS Omega*, 2019, **4**, 6175–6179.

57 J. Cheng, Z. Zhang, L. Zhang, J. Miao, Y. Chen, R. Zhao, M. Liu, L. Chen and X. Wang, *Talanta*, 2023, **257**, 124358.

58 N. Phuong, U. Nguyen, N. T. Dang and L. Doan, *Processes*, 2023, **11**, 2617.

59 C. Tian, L. Zhao, J. Zhu and S. Zhang, *J. Hazard. Mater.*, 2021, **416**, 126251.

60 Z. Zeng, Y. Liu and J. Wei, *TrAC, Trends Anal. Chem.*, 2016, **75**, 162–173.

61 M. Gambucci, E. Cambiotti and P. Sassi, *Molecules*, 2020, **25**, 3405.

62 M. Chen, D. Liu, X. Du, K. Ho, S. Wang, B. Zhou and H. Pan, *Trends Anal. Chem.*, 2020, **130**, 115983.

63 J. Zhou, T. Yang, J. Chen, C. Wang, H. Zhang and Y. Shao, *Coord. Chem. Rev.*, 2020, **410**, 213218.

64 Y. Chen, Y. Hu and L. Gongke, *Chemosensors*, 2023, **11**, 427.

65 J. Chen, K. Sun, Y. Zhang, D. Wu, Z. Jin, F. Xie, X. Zhao and X. Wang, *Anal. Bioanal. Chem.*, 2019, **411**, 2781–2791.

66 H. Sun, S. Cong, Z. Zheng, Z. Wang, Z. Chen and Z. Zhao, *J. Am. Chem. Soc.*, 2019, **141**, 870–878.

67 B. Soundiraraju and B. K. George, *ACS Nano*, 2017, **11**, 8892–8900.

68 Z. Yang, C. Ma, J. Gu, Y. Wu, C. Zhu, L. Li and H. Gao, *Spectrochim. Acta, Part A*, 2022, **267**, 120534.

69 C. Fu, S. Jin, W. Shi, J. Oh, H. Cao and Y. M. Jung, *Anal. Chem.*, 2018, **90**, 13159–13162.

70 S. E. J. Bell, G. Charron, E. Cortés, J. Kneipp, M. L. Chapelle, J. Langer, M. Procházka, V. Tran and S. Schlücker, *Angew. Chem., Int. Ed.*, 2020, **59**, 5454–5462.

71 L. Guerrini and R. A. Alvarez-puebla, *ACS Omega*, 2021, **6**, 1054–1063.

72 E. Chung, R. Gao, J. Ko, N. Choi, D. W. Lim, E. K. Lee, S. Chang and J. Choo, *Lab Chip*, 2013, **13**, 260–266.

73 C. Liu, H. Wang, S. Xu, H. Li, Y. Lu and C. Zhu, *Chemosensors*, 2023, **11**, 347.

74 S. Sarkar, M. Pradhan, A. K. Sinha and M. Basu, *Chem. – Eur. J.*, 2012, **18**, 6335–6342.

75 J. N. Lea, H. J. Montgomery, Y. Xu, S. E. J. Bell, L. Ashton and N. C. Fletcher, *Chem.: Methods*, 2023, **4**, e202300032.

76 S. Yan, F. Chu, H. Zhang, Y. Yuan, Y. Huang, A. Liu, S. Wang, W. Li, S. Li and W. Wen, *Spectrochim. Acta, Part A*, 2019, **220**, 117113.

77 H. Yuan, W. Ji, S. Chu, Q. Liu, S. Qian, J. Guang, J. Wang, X. Han, J. Masson and W. Peng, *ACS Sens.*, 2019, **4**, 704–710.

78 Y. Yang, K. Yook and J. Tae, *J. Am. Chem. Soc.*, 2005, **127**, 16760–16761.

79 J. Tao, S. Chen, E. Kouadio, W. Deng and D. Li, *Chem. Eng. J.*, 2023, **452**, 139026.

80 M. M. Hassan, W. Ahmad, M. Zareef, Y. Rong, Y. Xu, T. Jiao, P. He, H. Li and Q. Chen, *Food Chem.*, 2021, **358**, 129844.

81 H. Zhang, B. Wang, X. Liu, H. Zhang and J. Yan, *J. Appl. Spectrosc.*, 2022, **89**, 974–983.

82 L. Guerrini, I. Rodriguez, M. A. Correa-duarte, L. Guerrini, I. Rodriguez-loureiro, M. A. Correa-duarte, Y. H. Lee, Y. Ling and F. J. Garc, *Nanoscale*, 2014, **6**, 8368–8375.

83 J. A. Huang, Y. L. Zhang, H. Ding and H. B. Sun, *Adv. Opt. Mater.*, 2015, **3**, 618–633.

84 P. Zheng, X. Shi, K. Curtin, F. Yang and N. Wu, *Mater. Res. Express*, 2017, **4**, 055017.

85 C. C. Huang and H. T. Chang, *Chem. Commun.*, 2007, 1215–1217.

86 N. Feng, J. Shen, C. Li, Q. Zhao, E. K. Fodjo, L. Zhang, S. Chen, Q. Fan and L. Wang, *Analyst*, 2022, **147**, 1866–1872.

87 L. Xu, H. Yin, W. Ma, H. Kuang, L. Wang and C. Xu, *Biosens. Bioelectron.*, 2015, **67**, 472–476.

88 A. Yuan, X. Wu, X. Li, C. Hao, C. Xu and H. Kuang, *Small*, 2019, **15**, 1901958.

89 M. Liu, Z. Wang, S. Zong, H. Chen, D. Zhu, L. Wu, G. Hu and Y. Cui, *ACS Appl. Mater. Interfaces*, 2014, **6**, 7371–7379.

90 C. Liu, Y. Hsieh, C. Huang, Z. Lin and H. Chang, *Chem. Commun.*, 2008, 2242–2244.

91 K. A. Altammar, *Front. Microbiol.*, 2023, **14**, 1155622.

92 L. Long, W. Ju, H. Yang and Z. Li, *ACS Mater. Au*, 2022, **2**, 552–575.

93 N. R. Visaveliya, R. Mazetyte-Stasinskiene and J. M. Köhler, *Adv. Opt. Mater.*, 2022, **10**, 2102001.

94 Y. Tan, K. Yang, X. Zhang, Z. Zhou, Y. Xu, A. Xie and C. Xue, *ACS Omega*, 2023, **8**, 14541–14548.

95 S. HaiYang, W. Zhengkun, Z. Yong and Z. Jie, *Opt. Express*, 2023, **31**, 16484.

96 X. Li, G. Yuan, W. Yu, J. Xing, Y. Zou, C. Zhao, W. Kong, Z. Yu and C. Guo, *Lab Chip*, 2020, **20**, 414–423.

97 S. Guddala, S. A. Kamanoor, A. Chiappini, M. Ferrari and N. R. Desai, *J. Appl. Phys.*, 2012, **112**, 084303.

98 H. Wang, Y. Wu and H. Song, *Appl. Surf. Sci.*, 2019, **476**, 587–593.

99 E. Han, M. Zhang, Y. Pan and J. Cai, *Materials*, 2022, **15**, 2809.

100 G. P. Szekeres and J. Kneipp, *Front. Chem.*, 2019, **7**, 30.

101 C. Cheng, J. Li, H. Lei and B. Li, *Photonics Res.*, 2018, **6**, 357–362.

102 Y. Kalachyova, D. Mares, V. Jerabek, P. Ulbrich, L. Lapcak and O. Lyutakov, *Phys. Chem. Chem. Phys.*, 2017, **19**, 14761–14769.

103 X. Liu, M. Osada, K. Kitamura, T. Nagata and D. Si, *Sci. Rep.*, 2017, **7**, 3630.

104 Q. Zhao, H. Zhang, H. Fu, Y. Wei and W. Cai, *J. Hazard. Mater.*, 2020, **398**, 122890.

105 M. G. Ellis, U. Pant, J. Lou-franco, N. Logan and C. Cao, *ACS Appl. Nano Mater.*, 2023, 10431–10440.

106 Z. Chen, X. Su, H. Luo, A. Ade, H. Zhu, Y. Zhang and L. Yu, *Mater. Chem. Phys.*, 2023, **309**, 128335.

107 J. Li, W. Peng, A. Wang, M. Wan, Y. Zhou, X. G. Zhang, S. Jin and F. L. Zhang, *Analyst*, 2023, **148**, 4044–4052.

108 L. Yao, Y. Chen, R. Wang, C. Yan, J. Xu, B. Yao, J. Cheng and W. Chen, *Analyst*, 2022, **147**, 4337–4347.

109 Y. Lu, J. Zhong, G. Yao and Q. Huang, *Sens. Actuators, B*, 2018, **258**, 365–372.

110 X. Zhao, S. Campbell, P. Z. El-khoury, Y. Jia, G. Q. Wallace, A. Claing, C. G. Bazuin and J. Masson, *ACS Sens.*, 2021, **6**, 1649–1662.

111 Y. Wang, G. Wen, L. Ye, A. Liang and Z. Jiang, *Sci. Rep.*, 2016, **6**, 19650.

112 O. Guselnikova, V. Svorcik, O. Lyutakov and M. M. Chehimi, *Sensors*, 2019, **19**, 2110.

113 Y. Zhao, Y. Yamaguchi, Y. Ni, M. Li and X. Dou, *Spectrochim. Acta, Part A*, 2020, **233**, 2–7.

114 M. M. Lazar, C. Ghiorghita, E. S. Dragan, D. Humelnicu and M. V. Dinu, *Molecules*, 2023, **28**, 2798.

115 S. Gong, Y. Liang, X. Liu, H. Gao, H. Liao, X. Lin, M. Hasan, X. Zhou and S. Gunasekaran, *Appl. Surf. Sci. Adv.*, 2023, **18**, 100514.

116 M. Firouzzare and Q. Wang, *Talanta*, 2012, **101**, 261–266.

117 E. Ratnaningsih, G. T. M. Kadja, R. M. Putri, A. Alni, K. Khoiruddin, M. C. Djunaidi, S. Ismadji and I. G. Wenten, *ACS Omega*, 2022, **7**, 23009–23026.

118 I. Ahmad, W. A. Siddiqui, S. Qadir and T. Ahmad, *J. Mater. Res. Technol.*, 2018, **7**, 270–282.

119 C. Branger, W. Meouche and A. Margaillan, *React. Funct. Polym.*, 2013, **73**, 859–875.

120 L. Ye, P. A. G. Cormack and K. Mosbach, *Anal. Chim. Acta*, 2001, **435**, 187–196.

121 C. F. das V. Barros, J. de V. Cardoso and J. D. S. Castro, *Polym. J.*, 2023, **288**, 126424.

122 M. P. Rodríguez-reino, R. Rodríguez-fernández, E. Pe, R. Domínguez-gonzález, P. Bermejo-barrera and A. Moreda-pi, *J. Chromatogr. A*, 2015, **1391**, 9–17.

123 X. Luo, S. Luo, Y. Zhan, H. Shu, Y. Huang and X. Tu, *J. Hazard. Mater.*, 2011, **192**, 949–955.
124 B.-C. Iacob, A. E. Bodoki, L. Oprean and E. Bodoki, Metal–Ligand Interactions in Molecular Imprinting, *in* Ligand, ed. C. Saravanan and B. Biswas, Intech, 2018, DOI: 10.5772/intechopen.73407.
125 P. E. Hande, A. B. Samui and P. S. Kulkarni, *Environ. Sci. Pollut. Res.*, 2015, **22**, 7375–7404.
126 Ö Erdem, Y. Saylan, M. Andaç and A. Denizli, *Biomimetics*, 2018, **3**, 38.
127 N. Li and H. Yang, *J. Hazard. Mater.*, 2021, **403**, 123643.
128 M. Zougagh and A. Escarpa, *TrAC, Trends Anal. Chem.*, 2008, **27**, 54–65.
129 A. N. Hasanah, N. Safitri, A. Zulfa, N. Neli and D. Rahayu, *Molecules*, 2021, **26**, 5612.
130 X. Zhou, B. Wang and R. Wang, *Sep. Purif. Technol.*, 2022, **298**, 121469.
131 V. V. Kusumkar, M. Galamboš, E. Viglašov and M. Da, *Materials*, 2021, **14**, 1083.
132 I. Dakova, I. Karadjova, V. Georgieva and G. Georgiev, *Talanta*, 2009, **78**, 523–529.
133 W. Jiang, X. Jin, X. Yu, W. Wu, L. Xu and F. Fu, *J. Chromatogr. A*, 2017, **1496**, 167–173.
134 A. Bahrami, A. Besharati-seidani, A. Abbaspour and M. Shamsipur, *Mater. Sci. Eng., C*, 2015, **48**, 205–212.
135 N. Ain, S. Khairi, N. A. Yusof and A. H. Abdullah, *Int. J. Mol. Sci.*, 2015, **16**, 10562–10577.
136 M. Yasinzai, G. Mustafa, N. Asghar, I. Ullah, M. Zahid, P. A. Lieberzeit, D. Han and U. Latif, *J. Sens.*, 2018, **2018**, 8972549.
137 S. R. Thakare, M. R. Pal and S. Z. Jadhao, *Des. Monomers Polym.*, 2015, **18**, 650–660.
138 L. Mzukisi, N. Tawanda, H. Tutu and L. Chimuka, *Trends Environ. Anal. Chem.*, 2018, **17**, 14–22.
139 S. Khadijah, A. Rahman, N. A. Yusof, F. Mohammad, A. H. Abdullah and A. Idris, *Curr. Sci.*, 2017, **113**, 2282–2291.
140 M. J. Whitcombe and I. A. Nicholls, *J. Mol. Recognit.*, 2014, **27**, 297–401.
141 Y. Liu, Y. Zai, X. Chang and Y. Guo, *Anal. Chim. Acta*, 2006, **575**, 159–165.
142 P. Fan and B. Wang, *J. Appl. Polym. Sci.*, 2010, **116**, 258–266.
143 T. Alizadeh, M. Reza and M. Zare, *Anal. Chim. Acta*, 2011, **689**, 52–59.
144 G. Vasapollo, R. Del Sole, L. Mergola, M. R. Lazzoi, A. Scardino, S. Scorrano and G. Mele, *Mol. Sci.*, 2011, **12**, 5908–5945.
145 A. Karmakar, S. Hazra and A. J. L. Pombeiro, *Coord. Chem. Rev.*, 2022, **453**, 214314.
146 Z. Liu, S. Huan, J. Jiang, G. Shen and R. Yu, *Talanta*, 2006, **68**, 1120–1125.
147 A. C. do Lago, C. Marchioni, T. V. Mendes, C. Wisniewski, P. S. Fadini and P. O. Luccas, *Appl. Spectrosc.*, 2016, 70, 1842–1850.
148 N. T. Hoai, D. Yoo and D. Kim, *J. Hazard. Mater.*, 2010, **173**, 462–467.
149 G. Z. Memon, S. Sarwar, F. Memon, M. Q. Samejo and A. G. M. Vasandani, *Asian J. Chem.*, 2017, **29**, 1229–1234.
150 R. L. Mesa, J. E. L. Villa, S. Khan, R. R. A. Peixoto, M. A. Morgano, M. D. P. T. Sotomayor and G. Picasso, *Nanomaterials*, 2020, **10**, 2541.
151 K. Yoshimatsu, K. Reimhult, A. Krozer, K. Mosbach, K. Sode and L. Ye, *Anal. Chim. Acta*, 2007, **584**, 112–121.
152 S. Khadijah, A. Rahman, N. A. Yusof, A. H. Abdullah, F. Mohammad, A. Idris and H. A. Al-lohedan, *PLoS One*, 2018, **13**, e0208242.
153 H. Yavuz, R. N. Say and A. Denizli, *Mater. Sci. Eng., C*, 2005, **25**, 521–528.
154 R. Mesa, S. Khan and M. D. P. T. Sotomayor, *Biosensors*, 2022, **12**, 376.
155 A. Shirzadmehr, A. Afkhami and T. Madrakian, *J. Mol. Liq.*, 2015, **204**, 227–235.
156 F. Abdollahi, A. Taheri and M. Shahmari, *Sep. Sci. Technol.*, 2019, **55**, 2758–2771.
157 Y. Liu, X. Chang, D. Yang, Y. Guo and S. Meng, *Anal. Chim. Acta*, 2005, **538**, 85–91.
158 X. Fu, X. Chen, Z. Guo, C. Xie, L. Kong, J. Liu and X. Huang, *Anal. Chim. Acta*, 2011, **685**, 21–28.
159 M. Ghanei-motlagh, M. Ali, A. Heydari, R. Ghanei-motlagh and V. K. Gupta, *Mater. Sci. Eng., C*, 2016, **63**, 367–375.
160 M. Andac, S. Mirel, S. Senel, R. Say, A. Ersöz and A. Denizli, *Int. J. Biol. Macromol.*, 2007, **40**, 159–166.
161 S. Santana, C. Francisco, W. Nei, I. Helena, S. Estevam, G. Cardoso, C. Silva, A. Felix, S. Luis, C. Ferreira, D. De Ciências, C. I. Programa, D. Pós-graduaç and R. S. Martins, *Microchem. J.*, 2019, **150**, 104075.
162 R. Das, K. K. Paul and P. K. Giri, *Appl. Surf. Sci.*, 2019, **490**, 318–330.
163 T. Velempini, K. Pillay, X. Y. Mbianda and O. A. Arotiba, *Electroanalysis*, 2018, **30**, 2612–2619.
164 T. Alizadeh, N. Hamidi, M. R. Ganjali and F. Rafiei, *Microchim. Acta*, 2018, **185**, 16.
165 P. E. Hande, A. B. Samui and P. S. Kulkarni, *Sens. Actuators, B*, 2017, **246**, 597–605.
166 H. Li, Y. Li, D. Wang, J. Wang, J. Zhang and W. Jiang, *Sens. Actuators, B*, 2021, **340**, 129955.
167 E. Najafi, F. Aboufazeli, H. Reza, L. Zadeh, O. Sadeghi and V. Amani, *Food Chem.*, 2013, **141**, 4040–4045.
168 S. Soman and A. P. V. Kala, *J. Polym. Res.*, 2021, **28**, 359.
169 D. N. Basir, M. A. Zulfikar and M. B. Amran, *Songklanakarin J. Sci. Technol.*, 2020, **42**, 1135–1141.
170 L. Mergola, S. Scorrano, E. Bloise, M. Pia, D. Bello, M. Catalano, G. Vasapollo and R. Del Sole, *Polym. J.*, 2016, **48**, 73–79.
171 F. Esmali, Y. Mansourpanah, K. Farhadi, S. Amani, A. Rasoulifard and M. Ulbricht, *Sep. Purif. Technol.*, 2020, **250**, 117183.
172 R. Beeram, K. R. Vepa and V. R. Soma, *Biosensors*, 2023, **13**, 328.
173 B. Yarahmadi, S. M. Hashemianzadeh and S. M. R. Milani Hosseini, *Sci. Rep.*, 2023, **13**, 12111.